Structural and Thermochemical Properties of Hydroxymethyl (CH 2 OH) Radicals and Cations Derived from Observations of B̃ 2 A‘(3p) ← X̃ 2 A‘‘ Electronic Spectra and from ab Initio C...

ARTICLE *in* THE JOURNAL OF PHYSICAL CHEMISTRY · DECEMBER 1996

Impact Factor: 2.78 · DOI: 10.1021/jp961399+

2 AUTHORS:

Russell Johnson
National Institute of Standards and Technolo...
77 PUBLICATIONS **1,272** CITATIONS
SEE PROFILE

Jeffrey W Hudgens
National Institute of Standards and Technolo...
135 PUBLICATIONS **2,251** CITATIONS
SEE PROFILE

Structural and Thermochemical Properties of Hydroxymethyl (CH_2OH) Radicals and Cations Derived from Observations of $\tilde{B}\ ^2A'(3p) \leftarrow \tilde{X}\ ^2A''$ Electronic Spectra and from *ab Initio* Calculations

Russell D. Johnson III*,† and Jeffrey W. Hudgens*,‡

Physical and Chemical Properties Division, Chemical Sciences and Technology Laboratory, National Institute of Standards and Technology, Gaithersburg, Maryland 20899

Received: May 14, 1996; In Final Form: August 6, 1996[⊗]

$\tilde{B}\ ^2A'(3p) \leftarrow \tilde{X}\ ^2A''$ spectra of the isotopically substituted hydroxymethyl radicals (CH_2OH, CH_2OD, CD_2OH, CD_2OD) were observed between 39 700 and 43 000 cm^{-1} by 2+1, 2+2, and 1+1 resonance-enhanced multiphoton ionization (REMPI) spectroscopy. Analyses of the vibrational hot bands in these spectra show that the ν_8 torsion modes and ν_9 CH_2-wag mode are strongly coupled and governed by nonharmonic potential energy functions; for example, for $^{12}CH_2{}^{16}OH(\tilde{X}\ ^2A'')$ we obtain $2\nu_8 = 846 \pm 6$ $cm^{-1}(1\sigma)$, $1\nu_9 = 234 \pm 5$ cm^{-1}, and $2\nu_9 = 615 \pm 6$ cm^{-1}. Using MP2/6-311G(2df,2p) *ab initio* calculations, we constructed the two-dimensional potential energy surfaces that govern the ν_8 torsion modes and ν_9 CH_2-wag in the $\tilde{X}\ ^2A''$ radical and the $\tilde{X}\ ^1A'$ cation core of the $\tilde{B}\ ^2A'(3p)$ Rydberg state. Energy levels calculated with these potential energy surfaces account for the REMPI bands originating from the ν_8 hindered rotor and the ν_9 CH_2-wag modes. The experimental and *ab initio* results lead to improved heat capacities and entropies ($S°_{298.15}(CH_2OH) = 244.170 \pm 0.018$ J (mol K)$^{-1}$). *Ab initio* CBS-QCI/APNO calculations predict that $\Delta_f H°_{298.15}(CH_2OH) = -18.4 \pm 1.3$ kJ mol^{-1}. Re-evaluation of photoionization data yields $IP_a(CH_2OH) = 7.562 \pm 0.004$ eV. Re-evaluated photoionization appearance data, kinetic equilibrium data, and shock tube data indicate that $\Delta_f H°_0(CH_2OH^+) = 718.1 \pm 1.8$ kJ mol^{-1}, $\Delta_f H°_{298.15}(CH_2OH^+) = 716.4 \pm 1.8$ kJ mol^{-1}, $\Delta_f H°_0(CH_2OH) = -11.5 \pm 1.3$ kJ mol^{-1}, and $\Delta_f H°_{298.15}(CH_2OH) = -17.8 \pm 1.3$ kJ mol^{-1}. We report the proton affinity, $PA_0(CH_2O) = 705.2 \pm 1.9$ kJ mol^{-1}. Thermochemical tables based upon these values are presented for CH_2OH and CH_2OH^+.

I. Introduction

Over 100 papers have described the spectroscopic properties,[1−45] reaction mechanisms and kinetics,[3,6,8,9,15,21,24,25,29,30,37,38,42,46−87] thermochemistry,[10,17,18,45,47,50,59,78−80,83,88−99] and *ab initio* calculations[13,22,61,89,93,94,96,97,100−127] of the hydroxymethyl (CH_2OH) radical and cation. These studies were motivated by the important roles that CH_2OH and its isomer, CH_3O, play in the combustion of hydrocarbon fuels, atmospheric pollution chemistry, surface science, and interstellar chemistry. Examination of this current literature reveals that several fundamental properties lie in contention. In particular, the heats of formation for the CH_2OH radical, $\Delta_f H°_{298}(CH_2OH)$, derived from kinetic equilibria of neutral reactants are consistently 5−11 kJ mol^{-1} greater than those obtained from ion appearance energy data. Since calculations of $\Delta_f H°_{298}(CH_2OH)$ rely upon heat capacities and entropies estimated from spectroscopic data, we hypothesized that previous spectroscopic studies had overlooked the lowest energy vibrational states of the CH_2OH radical. During this study we observed these elusive, lowest energy ($E_v < 400$ cm^{-1}) vibrational levels as hot bands in the $\tilde{B}\ ^2A'(3p) \leftarrow \tilde{X}\ ^2A''$ resonance-enhanced multiphoton ionization (REMPI) spectra of thermal, isotopically selected, hydroxymethyl radicals. To refine the interpretation of our REMPI spectra, we performed extensive *ab initio* calculations of the hydroxymethyl radical and cation potential energy surfaces and calculated explicitly the energy levels of the coupled, nonharmonic vibrational modes. From these results we have prepared new tabulations of the thermochemical properties for the CH_2OH radical and cation. These improved thermochemical values differ significantly from previous ones and help to resolve the differences among the values of $\Delta_f H°_{298}(CH_2OH)$ derived from ion appearance energy and kinetic equilibrium data.

In 1983 our group reported the first electronic spectra of hydroxymethyl radicals.[3,4] Between laser wavelengths of 420 and 495 nm we observed the 2+1 REMPI spectra of isotopically substituted hydroxymethyl radicals and determined that their origins reside near 486.7 nm ($T_o = 41\ 060$ cm^{-1}). The identity of the upper state remained ambiguous until Dyke et al.[5] reported the photoelectron spectrum of CH_2OH and the adiabatic ionization potential, $IP_a(CH_2OH) = 7.56$ eV. In a subsequent paper on the vibrational analyses of isotopically substituted hydroxymethyl radicals this $IP_a(CH_2OH)$ allowed us to assign the upper state as a 3p Rydberg state.[6] *Ab initio* calculations by Rettrup et al.[110] have determined that the 2+1 REMPI spectrum of CH_2OH arises from promotion of an electron into the $3p_x$ Rydberg orbital; that is, the upper state is properly named $\tilde{B}\ ^2A'(3p)$ in the C_s point group (vide infra). Bomse et al.[7] have also reported 2+1 REMPI spectra of vibrationally excited CH_2OH and assigned part of the extensive hot band structure that appears near the origins. Pagsberg et al.[20,21] have reported ultraviolet absorption spectra of the $\tilde{A}\ ^2A'(3s) \leftarrow \tilde{X}\ ^2A''$ ($T_o = 35\ 050$ cm^{-1}) and $\tilde{B}\ ^2A'(3p) \leftarrow \tilde{X}\ ^2A''$ band systems. In this work we use the excellent sensitivity of REMPI spectroscopy[23,128−130] to expand upon the spectroscopic data by observing sparse populations of vibrationally excited ground state hydroxymethyl radicals.

REMPI spectra intrinsically juxtapose the disparate bonding within the (upper) Rydberg state and (lower) ground state radicals. Rydberg radicals of CH_2OH are described by the

† E-mail: russell.johnson@nist.gov. Fax: 301-975-3670.
‡ E-mail: jeffrey.hudgens@nist.gov. Fax: 301-926-3672.
⊗ Abstract published in *Advance ACS Abstracts,* December 1, 1996.

S0022-3654(96)01399-8 CCC: $12.00

configurations

$$...(\sigma_{CO})^2(\pi_{CO})^2(n_O)^2...(ns)^1$$
$$...(np)^1$$
$$...(nd)^1$$

where $n = 3, 4, 5, ...$ Rydberg orbitals are large and diffuse and contribute little to the bonding within the cationic molecular core. To a good approximation, the vibrational frequencies and structures of Rydberg radicals are the same as those exhibited by the ground state hydroxymethyl cation with the configuration

$$...(\sigma_{CO})^2(\pi_{CO})^2(n_O)^2 \qquad \tilde{X}\ ^1A'$$

Orbital considerations and *ab initio* calculations predict that the $CH_2OH^+(\tilde{X}\ ^1A')$ cation is planar and has a CO double bond.[114,115] Accordingly, the photoelectron[131] and REMPI spectra[3,6,7] of CH_2OH exhibit a characteristic CO double-bond stretching frequency of $\sim$1625 cm^{-1}. Self-consistent-field (SCF) calculations by Ha[115] estimate that the CO double bond produces a high torsional barrier of $\sim$9800 cm^{-1} that hinders the rotation of the hydrogen atom about the CO bond.

The higher occupied molecular orbitals of the hydroxymethyl radical are approximately described by the configuration

$$...(\sigma_{CO})^2(\pi_{CO})^2(n_O)^2(\pi^*_{CO})^1 \qquad \tilde{X}\ ^2A''$$

The half-occupied π^*_{CO} CO antibonding molecular orbital profoundly influences the structure and vibrational potential energy surface of $CH_2OH(\tilde{X}\ ^2A'')$ radicals. The most obvious effect is the reduced CO-stretch frequency of 1183 cm^{-1} observed in the infrared spectrum of matrix-isolated CH_2OH radicals.[1,2] Because the π^*_{CO} contribution does not remove all CO double-bond character, the CH_2OH radical has a modest barrier to internal rotation. From temperature dependent ESR measurements Krusic et al.[33] estimated that an activation energy of 1600 cm^{-1} hinders internal rotation. SCF calculations predict that the potential energy surface governing the ν_8 torsion mode has two unequal barriers of $B_\tau(\text{cis}) = 630$ cm^{-1} and $B_\tau(\text{trans}) = 1125$ cm^{-1}, where cis and trans refer to the position of the hydroxyl hydrogen relative to the methylene group.[115] More sophisticated MP3/6-31G**//6-31G** *ab initio* calculations by Saebø et al.[107] predict two equal barriers of $B_\tau = 1390$ cm^{-1}.

Electron spin resonance (ESR) studies show that $CH_2OH(\tilde{X}\ ^2A'')$ radicals maintain a pyramidal geometry about the carbon atom.[14,26−28,32−34] A pyramidal geometry occurs because distortion of the H_2-C-O geometry from planar to pyramidal geometries reduces the electron occupation of the π^*_{CO} orbital and lowers the the total energy of the radical. SCF calculations predict that the optimum pyramidal H_2-C-O geometry is about 140 cm^{-1} more stable than the optimum planar geometry.[115] MP3/6-31G**/6-31G** calculations estimate a difference of 320 cm^{-1}.[107]

The literature treatment of the ν_8 torsion mode and ν_9 CH_2-wag mode is remarkably inconsistent. Although ESR data[14,26−28,32−39,41] and *ab initio* calculations[107,115] suggest that nonharmonic potential energy surfaces govern the ν_8 torsion and ν_9 CH_2-wag modes of the CH_2OH radical, optical studies[3,4,6,7] and other *ab initio* studies[5,89,100,107] have treated these modes as harmonic oscillators. Previous reports have pointed out that inconsistent treatments of the torsion have impeded third-law determinations of $\Delta_f H°_{298}$ (CH_2OH).[47,90,92] Third-law determinations of $\Delta_f H°_{298}$ (CH_2OH) from kinetic equilibria require knowledge of the entropy, $S°_{298,15}$ (CH_2OH), which is calculated from the molecular partition function. Researchers have estimated the entropy of CH_2OH by assuming that (1) the torsion is a 420 cm^{-1} harmonic vibration ($S°_{298.15}$ $(CH_2OH) =$ 240.2 J $(mol\ K)^{-1}$),[90] (2) the torsion is a hindered rotor ($S°_{298.15}$ $(CH_2OH) = 242.2-245.6$ J $(mol\ K)^{-1}$),[92,132] and (3) the torsion is a free rotor ($S°_{298.15}$ $(CH_2OH) = 255.6$ J $(mol\ K)^{-1}$).[50,59] These diverse values of $S°_{298.15}$ (CH_2OH) have produced diverse evaluations of $\Delta_f H°_{298}$ (CH_2OH). For example, using the above entropies, different groups have evaluated Seetula and Gutman's data[50] for the reactions of Br and I with methanol. From the same kinetic equilibrium data they have derived values of $\Delta_f H°_{298}$ (CH_2OH) ranging from −9.1 kJ mol^{-1} to −14.7 kJ mol^{-1};[50,90,92] that is, a 15 J $(mol\ K)^{-1}$ variation of $S°_{298.15}$ (CH_2OH) induces a 5.6 kJ mol^{-1} variation of $\Delta_f H°_{298}$ (CH_2OH).

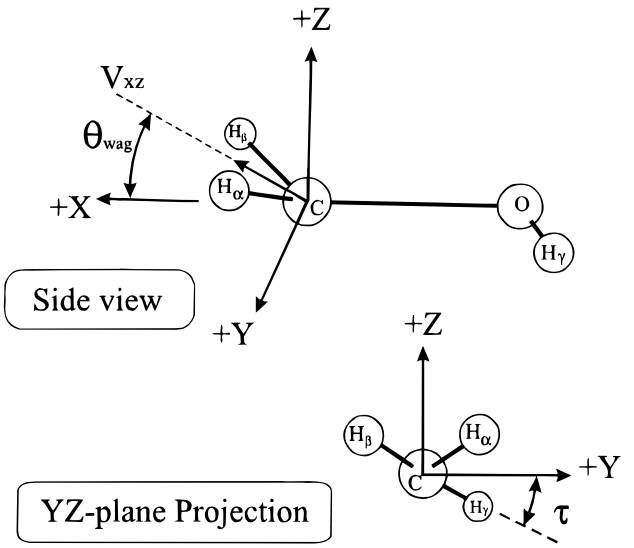

Figure 1. Two views of the coordinate system and geometric parameters of hydroxymethyl species. The *xz*-plane is orthogonal to the plane defined by $H_\alpha-C-H_\beta$. The vector, V_{xz}, is defined by the intersection of the *xz*-plane and the $H_\alpha-C-H_\beta$ plane. The CH_2-wag angle, θ_{wag}, is defined by the angle between V_{xz} and the positive *x*-axis. The torsion angle, τ, is the dihedral formed between the *xy*-plane and the $H_\gamma-O-C$ plane. When τ is negative, H_γ lies below the *xy*-plane.

II. Computational Methods and Results

a. Geometry and Potential Energy Surfaces. Figure 1 illustrates two views of the coordinate system and geometric parameters used in the discussions that follow. The origin of the coordinate system resides at the carbon atom. The C−O bond lies along the negative *x*-axis. The *xz*-plane is orthogonal to the plane defined by $H_\alpha-C-H_\beta$. As is shown in the side view, the vector, V_{xz}, is defined by the intersection of the *xz*-plane and the $H_\alpha-C-H_\beta$ plane. The CH_2-wag angle, θ_{wag}, is defined by the angle between V_{xz} and the positive *x*-axis. When θ_{wag} is negative, H_α and H_β lie below the *xy*-plane. As is shown in the projection onto the *yz*-plane, the torsion angle, τ, is the dihedral formed between the *xy*-plane and the $H_\gamma-O-C$ plane. When τ is negative, H_γ lies below the *xy*-plane.

Ab initio calculations on the hydroxymethyl radical and cation structures were performed using the GAUSSIAN 92 series of programs.[133,134] Table 1 presents one set of optimized geometries of the radical and cation obtained from calculations at the MP2/6-311G(2df,2p) level of theory. The values $\theta_{wag} = 0°$ and $\tau = 0°$ show that the cation is planar and belongs to the C_s point group. The radical structure contains the nonzero values $\theta_{wag} = 27.6°$ and $\tau = -7.4°$, indicating that the radical is nonplanar (Table 1). The methyl hydrogens, H_α and H_β, reside above the *xy*-plane, and the hydroxyl hydrogen, H_γ, resides below the *xy*-plane (Figure 1). Both species display unequal C−H bonds within the methylene group.

TABLE 1: Optimized Geometries of the Radical and Cation Obtained at the MP2/6-311G(2df,2p) Level

geometric parameter	radical[a]	cation[b]
r_{CO}, Å	1.3626	1.2463
$r_{OH\gamma}$, Å	0.9580	0.9803
$r_{CH\alpha}$, Å	1.0784	1.0858
$r_{CH\beta}$, Å	1.0746	1.0838
$\angle H_\alpha-C-H_\beta$, deg	120.5	122.8
$\angle O-C-H_\alpha$, deg	118.8	121.6
$\angle O-C-H_\beta$, deg	113.4	115.7
$\angle C-O-H_\gamma$, deg	108.4	115.1
$\angle V_{xz}-C-H_\alpha$, deg	57.0	58.4
$\angle V_{xz}-C-H_\beta$, deg	63.4	64.3
θ_{wag}, deg[c]	27.6[d]	0
τ, deg[e]	−7.4[d]	0

[a] Total energy of the optimized structure is −114.840 603 hartrees. 1 hartree = 219 474.7 cm^{-1}. [b] Total energy of the optimized structure is −114.577 437 hartrees. [c] θ_{wag} is defined in Figure 1. See text. [d] Four isoenergetic structures exist at $\tau = \mp 7.4°$, $\theta_{wag} = \pm 27.6°$ and $\tau = (180 \mp 7.4)°$, $\theta_{wag} = \pm 27.6°$. See text. [e] τ is defined in Figure 1. See text.

Figure 2 shows views of the two-dimensional potential energy surfaces that govern hydroxymethyl cations (panels a, b, c) and radicals (panels d, e, f). Each panel plots total energy as functions of τ, the coordinate of the ν_8 torsion mode, and θ_{wag}, the coordinate of the ν_9 CH_2-wag mode. Each potential energy surface is constructed from 1681 points. To calculate each point, we selected values for θ_{wag} and τ, and the molecular geometry was optimized at the MP2/6-311G(2df,2p) level. The energy range of the cation surface is 23 042 cm^{-1}. The energy range of the radical surface is 7920 cm^{-1}.

The cation's potential energy surface has 2-fold internal rotation symmetry with identical barriers of $B_\tau = 8331$ cm^{-1} located at $\tau = 90°$, $\theta_{wag} = 0°$ and at $\tau = -90°$, $\theta_{wag} = 0°$ (cf. Figure 2a). Two-fold rotation symmetry (along τ) is also found for any fixed value of θ_{wag} (cf. Figure 2c).

The radical's potential energy surface has 2-fold internal rotation symmetry with identical barriers of $B_\tau = 1643$ cm^{-1} located at $\tau = 90°$, $\theta_{wag} = -21°$ and at $\tau = -90°$, $\theta_{wag} = +21°$ (cf. Figure 2d). Rotations along the τ coordinate at constant θ_{wag} also exhibit 2-fold rotation symmetry (cf. Figure 2f). Along the CH_2-wag coordinate, θ_{wag}, the potential energy surface has two identical low barriers of $B_{wag} = 156$ cm^{-1} located at $\theta_{wag} = 0°$, $\tau = 0°$ and at $\theta_{wag} = 0°$, $\tau = 180°$. In Figure 2e this small barrier is barely visible. In fact, the structure shown in Table 1 is not unique but one of four isoenergetic structures. The potential energy surface has four isoenergetic minima located at two pairs of mirror image locations of $\tau = \mp 7.4°$, $\theta_{wag} = \pm 27.6°$ and $\tau = (180 \mp 7.4)°$, $\theta_{wag} = \pm 27.6°$.

b. Vibrational Symmetry and Mode Notation. At its equilibrium geometry the CH_2OH cation is planar and belongs to the C_s point group. The symmetry of the CH_2OH radical, if treated as a rigid body, is a member of the C_1 point group. However, because the CH_2OH radical has finite energy barriers, the mirror structures rapidly interconvert; therefore, its wave functions comply with the C_s point group. The highest occupied molecular orbital, π^*_{CO}, is singly occupied and is of a″ symmetry. Therefore, the ground state of the hydroxymethyl radical is properly designated $\tilde{X}\ ^2A''$.

The ν_8 torsion and the ν_9 CH_2-wag modes[135] of hydroxymethyl species involve out-of-plane motions. Both modes have a″ symmetry under the C_s point group. The other seven vibrational modes are in-plane motions of a′ symmetry. Furthermore, the 2-fold symmetry of the rotational barrier splits the torsional levels into + and − levels. Whenever required in this paper, we will label the ν_8 torsion quantum number with parity, e.g., 0^+, 0^-, 1^+, 1^-, 2^+, 2^-, ... (in conformance with practice in the infrared spectroscopy literature); otherwise, we will ignore the parity signs when designating the ν_8 torsion quantum numbers. In our spectra the minuscule splitting between these parity levels is not resolved.

TABLE 2: Moments of Inertia Used for Two-Dimensional Surface Vibrational Frequency Calculations

	torsion[a]				wag	
species	I^{calc}_{OH}, amu Å^2	$I^{calc}_{CH_2}$, amu Å^2	$I^{fit}_{torsion}$, amu Å^2	$I^{fit}_{torsion}$, amu Å^2	I^{calc}_{wag}, amu Å^2	I^{fit}_{wag}, amu Å^2
CH_2OH	0.832	1.877	0.576		0.468	
CH_2OD	1.663	1.877	0.882		0.468	
CD_2OH	0.832	3.751	0.681	0.695	0.818	0.666
CD_2OD	1.663	3.751	1.152	1.092	0.818	0.690

[a] The geometry used in determining the moments of inertia assumed equivalent C−H bond lengths and $r_{CH} = 1.0765$ Å, $r_{OH} = 0.958\ 04$ Å, $\theta_{wag} = 27.55°$, $\angle H-C-H = 120.0°$, and $\angle C-O-H = 108.45°$.

In these electronic spectra the vibrational selection rule, $\Delta v_n = 0, \pm 1, \pm 2, ...$, governs vibrational modes of a′ symmetry (i.e., modes ν_1 through ν_7) and the selection rule, $\Delta v_8 + \Delta v_9 = 0, \pm 2, \pm 4, ...$, governs vibrational modes of a′ symmetry (i.e., ν_8 and ν_9).

c. Vibrational Frequencies. As is well-known, the GAUSSIAN programs report harmonic vibrational frequencies. The program user must ascertain that each vibrational mode is well-approximated by a harmonic potential energy surface. Hydroxymethyl radicals and cations have seven vibrational modes, ν_1 through ν_7, that meet this approximation.

The ν_8 torsion and ν_9 CH_2-wag frequencies require more careful consideration. As noted above, the hydroxymethyl radical and cation possess isoenergetic mirror structures separated by finite barriers. Furthermore, as the hydroxyl group rotates about the C−O bond (by angle τ), geometry changes involving θ_{wag} and the bond lengths of the methyl hydrogens, may reduce the rotational barriers. These interactions may cause the ν_8 torsion mode to couple strongly to the ν_9 CH_2-wag mode. The frequency estimates provided by the GAUSSIAN routines are inappropriate and inaccurate. Instead, accurate estimates of the ν_8 torsion and ν_9 CH_2-wag frequencies are obtained from explicit calculations involving the two-dimensional potential energy surface.

Using the potential energy surfaces of Figure 2, we solved the two-dimensional vibrational eigenvalue problem using the Fourier grid Hamiltonian method.[136] This procedure yielded the vibrational energy levels of the combined ν_8 torsion and ν_9 CH_2-wag modes. Because we used angular displacements instead of Cartesian displacements, our method used moments of inertia instead of masses. The moments of inertia used to find the vibrational eigenvalues were arrived at as follows: The torsional moment of inertia, $I_{torsion}$, is a reduced moment of inertia involving the moment of inertia of H_γ about the line defined by the CO bond, I_{OH}, and the moment of inertia of H_α and H_β about the line defined by the CO bond, I_{CH2}. The reduced moment of inertia for torsion is given by the equation

$$I_{torsion} = \frac{1}{1/I_{OH} + 1/I_{CH2}} \qquad (1)$$

I_{wag} is the moment of inertia of the H_α, H_β, and carbon atoms about an axis parallel to the y-axis and through the center of mass of the $H_\alpha-C-H_\beta$ group.

Table 2 lists numerical values for the moments of inertia used to calculate the ν_8 torsion and ν_9 CH_2-wag frequencies. The same inertias were used for the radical and cation calculations. The calculated inertias accurately predict the experimental

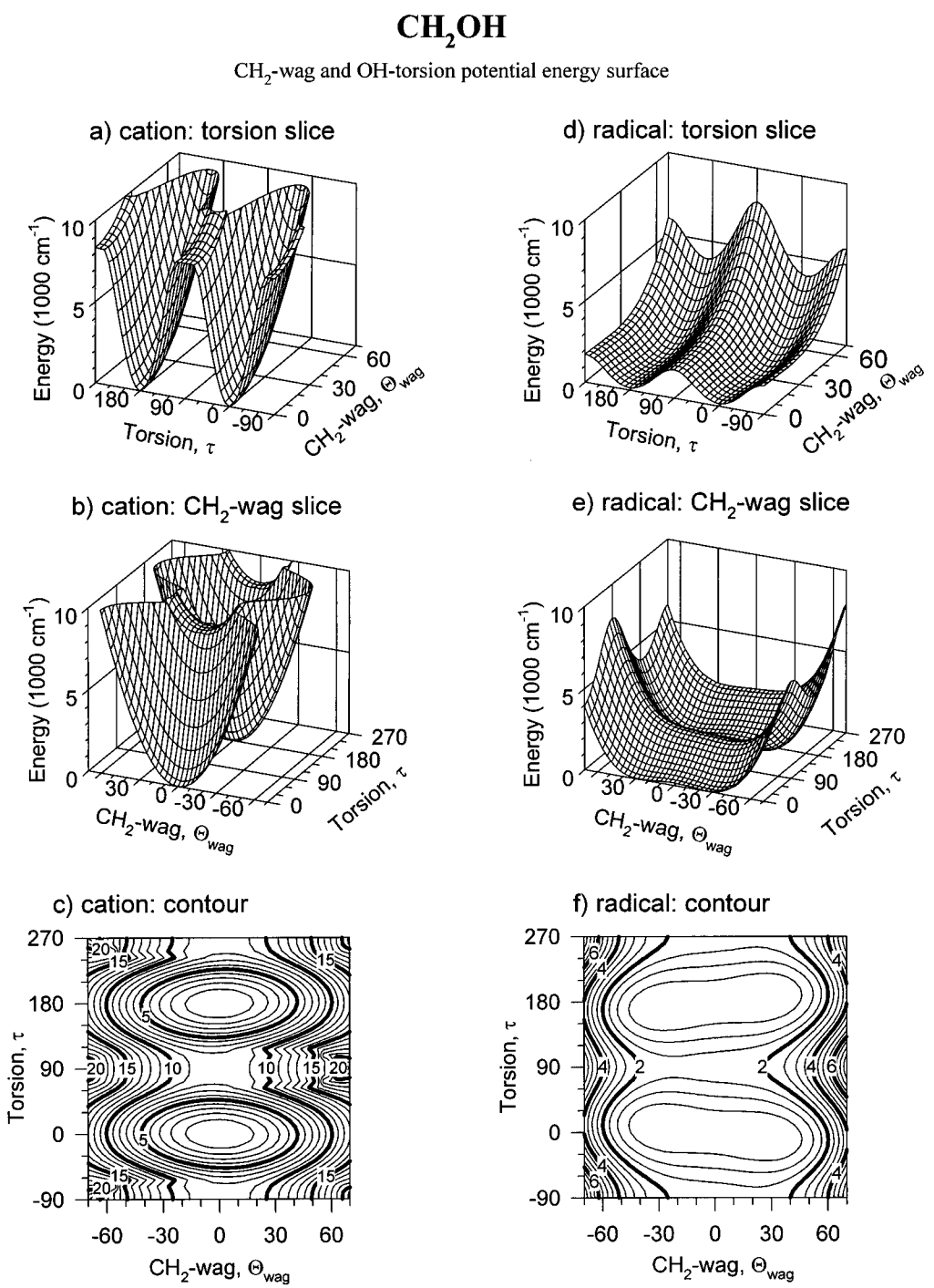

Figure 2. Views of the two-dimensional potential energy surfaces that govern hydroxymethyl cations (panels a, b, c) and radicals (panels d, e, f). Each panel plots total energy as functions of τ, the action coordinate of the ν_8 torsion mode, and θ_{wag}, the action coordinate of the ν_9 CH_2-wag mode. Energies are in units of 1000 cm^{-1}. Angles are in degrees. Each potential energy surface is constructed from 1681 optimized points at the MP2/6-311G(2df,2p) level. See the text.

spectroscopic data (presented below) of CH_2OH and CH_2OD species. To obtain a better fit of the spectroscopic data for CD_2-OH and CD_2OD, we used a least squares procedure that adjusted I^{fit}_{wag} and $I^{fit}_{torsion}$ to fit the 8^0_2, 9^0_2, and $8^0_1 9^0_1$ bands. Table 2 lists these fitted inertias. Each fitted inertia, I^{fit}_{wag}, differs significantly from calculated inertia, I^{calc}_{wag}. The differences between I^{calc}_{wag} and I^{fit}_{wag} arise because our model imperfectly describes the mechanical path of the ν_9 CH_2-wag motion within the heavier molecules.

Table 3 lists the fundamental vibrational frequencies of isotopically selected hydroxymethyl cations. To account for the overestimations of frequencies at this level of theory, the ν_1 through ν_7 frequencies are GAUSSIAN 92 values scaled by 0.97. The ν_8 torsion and ν_9 CH_2-wag frequencies listed in Table 3 were obtained from explicit calculations involving the two-dimensional potential energy surface. For all isotopomers these explicit calculations yield vibrational frequencies for the ν_8 torsion and ν_9 CH_2-wag modes that are ~5% lower than the scaled GAUSSIAN 92 harmonic frequencies.[137] Table 3 also lists ZPE (ν_8,ν_9), the zero-point-energy contribution of the ν_8 and ν_9 modes, and ZPE, the total zero-point energy of each cation.

For comparison purposes Table 3 lists vibrational frequencies of hydroxymethyl cations derived from experiments. Table 3 also lists experimentally observed vibrational frequencies of Rydberg radicals which serve as surrogates of the cation. This

TABLE 3: Calculated and Experimental Vibrational Frequencies of Isotopomers of Hydroxymethyl Cation[135] (The Calculated Frequencies of Modes ν_1 through ν_7 Were Obtained at the MP2/6-311G(2df,2p) Level and Then Scaled by 0.97; the Vibrational Frequencies of ν_8 and ν_9 Were Obtained from Explicit Calculation Using the Two-Dimensional Potential Energy Surface; See Text)

	CH_2OH^+		CH_2OD^+		CD_2OH^+		CD_2OD^+	
mode	ν_{calc}, cm^{-1}	ν_{obs}, cm^{-1}	ν_{calc}, cm^{-1}	ν_{obs}, cm^{-1}	ν_{calc}, cm^{-1}	ν_{obs}, cm^{-1}	ν_{calc}, cm^{-1}	ν_{obs}, cm^{-1}
ν_1 (a′) OH stretch	3511	3422.8024[a]	2561		3510		2561	
ν_2 (a′) CH_2 asym str	3214		3214		2413		2412	
ν_3 (a′) CH_2 sym str	3068		3068		2242		2241	
ν_4 (a′) CH_2 scissors	1463	1459,[b] 1465[c]	1457	1440,[b] 1446[c]	1077	1094,[b] 1068[c]	1068	1093[c]
ν_5 (a′) in-phase HCOH bend	1356	1351,[b] 1357,[c] 1370[d]	868		1276	1298[b]	1086	1109[b]
ν_6 (a′) CO stretch	1643	1623,[b] 1621,[c] 1650[d]	1636	1612[b]	1576	1568[b]	1567	1565[b]
ν_7 (a′) out-of-phase HCOH bend	1092	1091,[b] 1107[c]	1277	1296[b]	897	909[b]	787	
ν_8 (a″) torsion	978[e]	993[c]	794[e]	800[c]	888[e]	885[c]	715[e]	723[c]
ν_9 (a″) CH_2 wag	1175[e]		1173[e]	1170[c]	990[e]	994[c]	968[e]	952[c]
ZPE(ν_8,ν_9)	1083[e]		989[e]		945[e]		845[e]	
ZPE[f]	8757		8030		7441		6706	

[a] Vibrational frequency of the cation from ref 19. Stated accuracy is ±0.0007 cm^{-1}. [b] Vibrational frequency of $\tilde{B}\ ^2A'(3p)$ Rydberg state reported in ref 6. Accuracy is ±5 cm^{-1}. [c] Vibrational frequency of the $\tilde{B}\ ^2A'(3p)$ Rydberg state from this study. See Table 13. [e] From explicit calculation of the two-dimensional potential energy surface of the cation. See text. [f] The zero-point energy is calculated using ZPE = $^1/_2\sum_{n=1}^{7}\nu_n$ + ZPE(ν_8,ν_9). [d] Vibrational frequency of the cation from ref 5. Stated accuracy is ±30 cm^{-1}.

TABLE 4: Spectroscopic Constants for Hydroxymethyl Cations That Describe Manifolds of ν_8 Torsion and ν_9 CH_2-Wag Vibrational Energy Levels ($E_v^{limit}(\nu_8,\nu_9)$ Is the Upper Limit for Which These Constants Are Valid; the Parity Levels of the ν_8 Torsion Mode Are Ignored; See Text)

spectroscopic constant[a]	CH_2OH	CH_2OD	CD_2OH	CD_2OD
ω_8, cm^{-1}	995.16	805.62	903.44	729.15
x_8, cm^{-1}	−8.8124	−3.351	−7.240	−1.743
ω_9, cm^{-1}	1181.48	1179.65	994.34	968.12
x_9, cm^{-1}	−3.3767	−5.566	−2.574	−5.935
x_{89}, cm^{-1}	−0.9597	−1.13	−0.983	−0.157
$E_v^{limit}(\nu_8,\nu_9)$, cm^{-1}	5741	5276	5838	4192

[a] $E_v(\nu_8,\nu_9) = \omega_8(\upsilon_8 + {}^1/_2) + x_8(\upsilon_8 + {}^1/_2)^2 + \omega_9(\upsilon_9 + {}^1/_2) + x_9(\upsilon_9 + {}^1/_2)^2 + x_{89}(\upsilon_8 + {}^1/_2)(\upsilon_9 + {}^1/_2)$.

is appropriate because Rydberg radicals and the $\tilde{X}\ ^1A'$ cation share the same molecular valence core. Overall, the calculated and the observed vibrational frequencies of hydroxymethyl cations are in good agreement.

The two-dimensional potential energy surface enables calculations of the manifold ν_8 torsion and ν_9 CH_2-wag vibrational energy levels of the cation. For derivation of thermochemical properties we calculated the first 428 eigenvalues up to $E_v(\nu_8,\nu_9)$ = 19 916 cm^{-1}. For $E_v(\nu_8,\nu_9)$ < 5000 cm^{-1} the vibrational eigenvalues are nearly degenerate pairs of + and − parity states separated by $<10^{-4}$ cm^{-1}. As $E_v(\nu_8,\nu_9)$ approaches the torsion barrier, the parity states separate into distinct vibrational levels with separations that vary from 0.1 to 5 cm^{-1}.

In the cations the lower levels of the ν_8 and ν_9 vibrational manifold align into nearly harmonic patterns fit by standard formulas. For each cation isotopomer Table 4 lists these spectroscopic constants and $E_v^{limit}(\nu_8,\nu_9)$, the energy above which the spectroscopic constants become invalid. Below $E_v^{limit}(\nu_8,\nu_9)$ the spectroscopic constants fit the ν_8 and ν_9 vibrational energy levels with an accuracy of ±3 cm^{-1}. The small spectroscopic constants, x_{89}, indicate that the ν_8 torsion and ν_9 CH_2-wag modes are weakly cross-coupled. Above $E_v^{limit}(\nu_8,\nu_9)$ the ν_8 and ν_9 energy levels become less regularly spaced (although the parity levels remain nearly degenerate). The irregularities arise from the increased coupling between the ν_8 torsion and ν_9 CH_2-wag modes and from the anharmonicity induced by approaching and exceeding the potential energy barrier to internal rotation (B_τ = 8331 cm^{-1}).

A similar set of calculations predicted the vibrational frequencies of hydroxymethyl radicals. For each isotopic radical Table 5 lists the vibrational frequencies obtained for the harmonic vibrational modes (ν_1 through ν_7) and the ZPE. These values are harmonic frequencies reported by MP2/6-311G(2df,2p) GAUSSIAN 92 calculations[138] scaled by 0.94. Table 5 also lists the experimentally known vibrational frequencies.

For hydroxymethyl radicals Table 6 lists the lower vibrational energy levels of the ν_8 torsion and ν_9 CH_2-wag manifold and values of ZPE(ν_8,ν_9). These energy levels were obtained by explicit calculation over the two-dimensional potential energy surface (Figure 2d−f) using the inertias listed in Table 2. The patterns of energy levels of the ν_8 torsion and ν_9 CH_2-wag modes do not fit simple spectroscopic formulas. For Table 6 we determined the υ_8 and υ_9 quantum numbers for each level by visually examining the graph of each wave function. Even the lowest ν_8 and ν_9 energy levels of hydroxymethyl radicals contain large contributions from the torsion and CH_2-wag motions;

TABLE 5: Calculated and Observed Vibrational Frequencies of Hydroxymethyl Radicals[135] (The Calculated Frequencies Were Obtained at the MP2/6-311G(2df,2p) Level and Scaled by 0.94; See Text)

	CH_2OH		CH_2OD		CD_2OH		CD_2OD	
mode	ν_{calc}, cm^{-1}	ν_{obs}, cm^{-1}	ν_{calc}, cm^{-1}	ν_{obs}, cm^{-1}	ν_{calc}, cm^{-1}	ν_{obs}, cm^{-1}	ν_{calc}, cm^{-1}	ν_{obs}, cm^{-1}
ν_1 (a′) OH stretch	3681	3650,[a] 3637[b]	2680	2695[a]	3681	3650[a]	2680	2682,[b] 2694[a]
ν_2 (a′) CH_2 asym str	3159		3160		2362		2361	
ν_3 (a′) CH_2 sym str	3019		3019		2183		2183	
ν_4 (a′) CH_2 scissors	1432	1459[a]	1432		992	1019,[a] 1019[c]	990	1041,[a] 1020[c]
ν_5 (a′) in-phase HCOH bend	1311	1334[a]	1188		1258		1016	
ν_6 (a′) CO stretch	1165	1183,[b,a] 1176[c]	1163	1183,[a] 1178[c]	1197	1213,[a] 1208[c]	1205	1222,[b] 1223,[a] 1221[c]
ν_7 (a′) out-of-phase HCOH bend	1017	1056,[b] 1048[a]	832	861,[a] 864[c]	815	842[a]	738	765[a]
ZPE[d]	7571	7600	6900		6402		5725	

[a] From Ar matrix study of ref 1. [b] From N_2 matrix study of ref 2. [c] This work. [d] The zero-point energy is calculated using ZPE = $^1/_2\sum_{n=1}^{7}\nu_n$ + ZPE(ν_8,ν_9), where ZPE(ν_8,ν_9) is listed in Table 6.

TABLE 6: Vibrational Energy Levels and Zero-Point Energies of the ν_8 Torsion and ν_9 CH_2-Wag Modes of Hydroxymethyl Radicals Obtained from a Two-Dimensional Potential Energy Surface Computed with MP2/6-311G(2df,2p) Level Calculations

CH_2OH				CH_2OD				CD_2OH				CD_2OD			
ν_{calc}, cm^{-1}	ν_{obs},[a] cm^{-1}	υ_8 tors	υ_9 wag	ν_{calc}, cm^{-1}	ν_{obs},[a] cm^{-1}	υ_8 tors	υ_9 wag	ν_{calc}, cm^{-1}	ν_{obs},[a] cm^{-1}	υ_8 tors	υ_9 wag	ν_{calc}, cm^{-1}	ν_{obs},[a] cm^{-1}	υ_8 tors	υ_9 wag
0		0^+	0	0		0^+	0	0		0^+	0	0		0^+	0
0		0^-	0	0		0^-	0	0		0^-	0	0		0^-	0
238	234 ± 5	0^+	1	227	223 ± 9	0^+	1	174	221 ± 9	0^+	1	161	177 ± 23	0^+	1
238		0^-	1	227		0^-	1	174		0^-	1	161		0^-	1
418	420[b]	1^+	0	367	353 ± 9	1^+	0	375	347 ± 9	1^+	0	311	329 ± 23	1^+	0
418		1^-	0	367		1^-	0	375		1^-	0	311		1^-	0
607	616 ± 6, 607 ± 15[c]	0^+	2	540	550 ± 5	0^+	2	492	500 ± 4, 498 ± 15[c]	0^+	2	428	448 ± 4	0^+	2
607		0^-	2	540		0^-	2	492		0^-	2	428		0^-	2
734		1^+	1	671		1^+	1	602	595 ± 4	1^+	1	544	543 ± 5	1^+	1
734		1^-	1	671		1^-	1	602		1^-	1	544		1^-	1
839	846 ± 6	2^+	0	788	803 ± 5	2^+	0	737	735 ± 4	2^+	0	630	617 ± 4	2^+	0
840		2^-	0	788		2^-	0	737		2^-	0	630		2^-	0
976		0^+	3	851		0^+	3	831		0^+	3	701		0^+	3
978		0^-	3	852		0^-	3	831		0^-	3	701		0^-	3
1083		1^+	2	974		1^+	2	917		1^+	2	807		1^+	2
1089		1^-	2	975		1^-	2	917		1^-	2	807		1^-	2
1201		2^+	1	1122		2^+	1	1021	1021 ± 10	2^+	1	903	962 ± 25	2^+	1
1206		2^-	1	1122		2^-	1	1023		2^-	1	903		2^-	1
1294		0^+	4	1141	1143 ± 15	3^+	0	1108		3^+	0	968		0^+	4
1326		0^-	4	1146		3^-	0	1109		3^-	0	969		0^-	4
1361		3^+	0	1262		0^+	4	1159		0^+	4	1017		3^+	0
1362		3^-	0	1268		0^-	4	1163		0^-	4	1017		3^-	0
1400		1^+	3	1336				1232		1^+	3	1067	(1044 ± 12)[d]	1^+	3
1431		1^-	3	1337				1242		1^-	3	1068		1^-	3
1512		0^+	5	1377				1321		2^+	2	1171		2^+	2
1556		2^+	2	1417				1335		2^-	2	1172		2^-	2
1570		2^-	2	1441				1420		0^+	5	1216		0^-	5
1653		0^-	5	1445				1424		0^-	5	1221		0^-	5
1685		1^+	4	1523				1430		3^+	1	1308		3^+	1
1730		2^+	4	1546				1472		3^-	1	1308		3^-	1
1749		3^-	1	1548				1506				1309		1^+	4
1751		3^+	1	1676				1553				1315		1^-	4
1762		1^-	4	1679				1554				1419		0^+	6
1897		2^+	3	1680				1556				1431			
1910		1^+	5	1713				1607				1435		2^+	3
1925		2^-	3	1753				1620							
$ZPE(\nu_8,\nu_9) = 358$ cm^{-1}				$ZPE(\nu_8,\nu_9) = 326$ cm^{-1}				$ZPE(\nu_8,\nu_9) = 315$				$ZPE(\nu_8,\nu_9) = 277$ cm^{-1}			

[a] Derived from the spectra of this study unless noted otherwise. See Table 13. [b] Ar matrix data of ref 1. [c] Reinterpretation of data from the gas phase study of ref 7. See text. [d] Based on a tentative assignment. See Table 12.

therefore, classifications of eigenfunctions with the terms "torsion" or "CH_2-wag" is approximate. For the vibrational energy levels that reside near the torsional barrier, the strong coupling between the modes produces complex nodal patterns and the υ_8 and υ_9 quantum number assignments become ambiguous. In Table 6 these ambiguous energy levels are not labeled. Moreover, as the torsional barrier is approached, the parity levels exhibit significant separations.

Table 6 also lists experimentally observed ν_8 and ν_9 vibrational energy levels. Most of these experimental values were derived from analyses of the REMPI spectra presented below. For derivation of the thermochemical properties of hydroxymethyl radicals, we calculated the first 837 eigenvalues up to $E_v(\nu_8,\nu_9) = 29\,410$ cm^{-1}.

d. Franck−Condon Factors. The calculational procedure that finds the vibrational eigenvalues for the combined ν_8 and ν_9 modes also obtains the eigenvectors. The dot product of the radical and cation eigenvectors gives the relative Franck−Condon factors for transitions between selected ν_8 and ν_9 vibrational levels. These Franck−Condon factors predict the relative strength of transitions between the ground and Rydberg states. Table 7 lists relative transition strengths normalized so that the strongest transition (the origin band) is 100. Table 7 also lists the relative Boltzmann population of the quantum levels at 298 K. The predicted line strength (not listed) is the product of the Franck−Condon factors and the vibrational distribution functions. (Table 7 does not list this predicted line strength because our reaction temperature is unknown and energy transfer processes may have caused the population distribution to deviate from Boltzmann.)

As discussed above, the 2-fold symmetry in the ν_8 torsion mode produces practically degenerate vibrational states. As a result, the origin band is comprised of four $(\upsilon_8' + \upsilon_9') \leftarrow (\upsilon_8'' + \upsilon_9'')$ transitions: $0^+ \leftarrow 0^+$, $0^+ \leftarrow 0^-$, $0^- \leftarrow 0^+$, and $0^- \leftarrow 0^-$. The $0^+ \leftarrow 0^-$ and $0^- \leftarrow 0^+$ transitions are symmetry forbidden; so these Franck−Condon factors are zero. The individual Franck−Condon factor of the $0^+ - 0^+$ transition is 0.66. This value is used to normalize Franck−Condon factors in Table 7. We note that the combination bands $8_0^1 9_1^0$ and $8_1^0 9_0^1$ carry appreciable intensity. These off-diagonal Franck−Condon factors are comparable to the diagonal 8_1^1 or 9_1^1 transitions.

e. Heat of Formation of CH_2OH Radical Derived from *ab Initio* Calculations. To obtain an accurate theoretical estimate of $\Delta_f H°_{298.15}(CH_2OH)$, we calculated the enthalpy of reaction for the isodesmic reaction

$$CH_2OH + CH_4 \rightarrow CH_3OH + CH_3 \qquad (2)$$

using the CBS-QCI/APNO protocol.[139] The use of isodesmic

TABLE 7: Relative Frank−Condon Factors for Transitions between the Radical and Cation Involving the ν_8 Torsion and ν_9 CH_2-Wag Modes

		υ_8''	0	0	1	0	1	2	0	1	2
		υ_9''	0	1	0	2	1	0	3	2	1
		sym	a′	a″	a″	a′	a′	a′	a″	a″	a″
		G″(υ_8,υ_9), cm^{-1}	0	238	418	607	734	839	976	1083	1201
υ_8'	υ_9'	sym	G′(υ_8,υ_9), cm^{-1}								
0	0	a′	0	100[a] 8_0^0		21 9_2^0	5 $8_1^0 9_1^0$	15 8_2^0			
1	0	a″	978	25 $8_0^1 9_1^0$	58 8_1^1				22 $8_0^1 9_3^0$	4 $8_1^1 9_2^0$	24 $8_2^1 9_1^0$
0	1	a″	1175	57 9_1^1	31 $8_1^0 9_0^1$				4 9_3^1	3 $8_1^0 9_2^1$	0 $8_2^0 9_1^1$
2	0	a′	1939	12 8_0^2		13 $8_0^2 9_2^0$	26 $8_1^2 9_1^0$	2 8_2^2			
1	1	a′	2151	2 $8_0^1 9_0^1$		30 $8_0^1 9_2^1$	8 $8_1^1 9_1^1$	33 $8_2^1 9_0^1$			
0	2	a′	2344	24 9_0^2		0 9_2^2	28 $8_1^0 9_1^2$	18 $8_2^0 9_0^2$			
rel pop[b]			1.00	0.45	0.20	0.13	0.09	0.06	0.04	0.03	0.02

[a] Franck−Condon factors have been multiplied by 100/0.66 to give relative FC factors normalized to 100. [b] Populations calculated for 300 K Boltzmann distribution.

TABLE 8: Determination of the Heat of Formation of CH_2OH from Zero-Point-Energy-Corrected CBS-QCI/APNO Calculations of the Isodesmic Reaction $CH_2OH + CH_4 \rightarrow CH_3OH + CH_3$

	CH_2OH	CH_4	CH_3OH	CH_3	computed value, kJ mol^{-1}
$\Delta_f H°_0$, kJ mol^{-1}	$\Delta_f H°_0(CH_2OH)$ ±0.53[a]	−66.91 ±0.8	−190.05 ±0.5	149.03 ±0.34	$\Delta_r H°_0 = [25.89 - \Delta_f H°_0(CH_2OH)] \pm 1.3$
H_0^{CBS}, hartree	−115.019 608	−40.468 957	−115.670 900	−39.803 893	$\Delta_r H_0^{CBS} = 36.16$ (0.013 772 hartree)
ZPE^{CBS}, cm^{-1}	8052	9530	11137	6173	
ZPE^{expt},[b] cm^{-1}	7600[c]	9480	10669[d]	6294[e]	
[$ZPE^{CBS} - ZPE^{expt}$], cm^{-1}	452	50	468	−121	$\Delta_r[ZPE^{CBS} - ZPE^{expt}] = -1.85$ (−155 cm^{-1})
	$\Delta_r H_0^{calc} - \Delta_r H°_0 = \Delta_r H_0^{CBS} - \Delta_r[ZPE^{CBS} - ZPE^{expt}] - [25.89 - \Delta_f H°_0(CH_2OH)]$				0
	$\Delta_f H°_0(CH_2OH)$				−12.1 ± 1.3
	heat correction[f]				−6.3
	$\Delta_f H°_{298.15}(CH_2OH)$				−18.4 ± 1.3

[a] Residual error estimated from a CBS-QCI/APNO calculation of reaction 3. See text. [b] Computed using values from refs 141, 142 unless noted otherwise. [c] From Table 5. [d] Includes torsion oscillator energy, $ZPE(\nu_{12}) = 128$ cm^{-1}, which is derived from Figure 1 of ref 143. [e] Includes quartic oscillator energy, $ZPE(\nu_2) = 235$ cm^{-1}. [f] Derived from Table 16.

reactions increases the accuracy of thermochemical estimates because the number of bonds and the bond types are preserved on both sides of the reaction. As a result, the computational errors associated with these species tend to cancel.[140]

Table 8 outlines this derivation, which uses CBS-QCI/APNO results and the experimentally known values $\Delta_f H°_0(CH_4)$, $\Delta_f H°_0(CH_3)$, and $\Delta_f H°_0(CH_3OH)$ to solve for $\Delta_f H°_0(CH_2OH)$. We calculate the *ab initio* heat of reaction 2, $\Delta_r H_0^{CBS}$, using the CBS-QCI/APNO total energy for each reactant, H_0^{CBS}. Each reactant's *ab initio* total energy, H_0^{CBS}, contains a zero-point energy, ZPE^{CBS}, calculated from harmonic vibrational frequencies. Since CH_2OH, CH_3OH, and CH_3 contain nonharmonic torsion or nonharmonic inversion modes, these values of ZPE^{CBS} are inaccurate. For each reactant Table 8 lists the more accurate ZPE^{expt} derived from experimental data[141−143] and [$ZPE^{CBS} - ZPE^{expt}$], the difference between the *ab initio* and experimental ZPEs. The ZPE corrections increase the endothermicity of reaction 2 by 1.85 kJ mol^{-1}. The overall calculation estimates that $\Delta_f H°_0(CH_2OH) = -12.1 \pm 1.3$ kJ mol^{-1}.[144] A heat correction is applied to obtain $\Delta H_f°_{298.15}(CH_2OH) = -18.4 \pm 1.3$ kJ mol^{-1}.

Test calculations over 64 first-row examples of the G2 test set have shown that the CBS-QCI/APNO method predicts bond dissociation energies with an absolute accuracy of ±2.2 kJ mol^{-1}.[139] To estimate the error in the predicted $\Delta H_f°_{298.15}(CH_2OH)$, we used the experimental uncertainty of $\Delta H_f°_0$ for each reagent and included the residual error that we expect of the isodesmic reaction (2) (Table 8). We appraise this residual error by assuming that it is the upper limit of error associated with the CBS-QCI/APNO calculation of the enthalpy for the reaction

$$CH_3OH + CO \rightarrow 2CH_2O \quad (3)$$

For the isogyric hydrogen transfer reaction (3) CBS-QCI/APNO calculations overestimate the exothermicity of reaction 3 by −0.3 kJ mol^{-1}, which is within the error limits of the experimentally determined reaction enthalpy (i.e., $1\sigma = \pm 0.53$ kJ mol^{-1}). Therefore, we adopted ±0.53 kJ mol^{-1} as the residual error of the isodesmic reaction (2).

III. Experimental Apparatus and Procedures

The apparatus used in this study has been described elsewhere.[145] Briefly, it consisted of a flow reactor that produced the free radical species, an excimer-pumped dye laser that irradiated the radicals and drove the multiphoton ionization process, a time-of-flight mass spectrometer, and a computer/data acquisition system. Free radicals produced in the flow reactor effused through a 0.2 mm diameter skimmer and into the ion source of the mass spectrometer, where they were ionized by a focused laser beam (2−10 mJ/pulse, 20 ns, 0.2 cm^{-1} fwhm, fl = 250 nm). Since the flow reactor was operated at pressures between 260 and 660 Pa (∼2−5 Torr), no expansion cooling occurred. The pressure within the ion source was about 9×10^{-3} Pa ($\sim 5 \times 10^{-5}$ Torr). The laser-generated ions were mass selected and detected by the mass spectrometer. The ion flight time that corresponded to the isotopically selected hydroxymethyl molecular ion was sampled by a gated integrator, and the ion signal was averaged, displayed, and recorded with a microcomputer.

The spectra consist of the mass specific ion current as a function of laser wavelength. Four isotopic precursors were used: CH_3OH (Burdick and Jackson, HPLC grade), CH_3OD

TABLE 9: Band Maxima Observed in the 2+1 (2+2) REMPI and 1+1 REMPI (*m/z* 31) Spectra of CH_2OH Radicals[135]

λ_{air}, nm	$2h\nu_{obs}$, cm^{-1}	$2h(\nu_{obs}-\nu_o)$, cm^{-1}	λ_{air}, nm	$1h\nu_{obs}$, cm^{-1}	$1h(\nu_{obs}-\nu_o)$, cm^{-1}	assignment
501.26	39 888	−1180	250.58	39 896	−1165	6_1^0
			249.49	40 070	−991	
496.98	40 230	−838	248.64	40 206	−855	8_2^0
499.09	40 457	−611	247.20	40 441	−620	9_2^0
			245.07	40 792	−269	
486.86	41 068	0	243.46	41 061	0	0_0^0
481.64	41 513	445				6_1^1
480.17	41 641	573				8_1^1
477.84	41 843	775				$6_0^1 8_2^0$
475.96	42 009	941				9_1^1
474.08	42 175	1107				7_0^1
471.29	42 425	1357				5_0^1
470.09	42 533	1465				4_0^1
468.37	42 689	1621				6_0^1

(Cambridge Isotope Labs, 99% OD), CD_3OH (Isotec, Inc. 95% CD_3), and CD_3OD (MSD Isotopes 99.6% D).[146]

IV. Experimental Results and Analyses of the REMPI Spectra

In the flow reactor fluorine was reacted with methanol to produce hydroxymethyl and methoxy radicals, e.g.,

$$\begin{aligned} F + CH_3OD &\rightarrow HF + CH_2OD \\ &\rightarrow DF + CH_3O \end{aligned} \qquad (4)$$

Previous experiments have established that methoxy radicals do not contribute REMPI bands in the spectral range of this study.[3,6] The reaction of each isotopically selected precursor produced a unique, isotopically substituted hydroxymethyl radical, which ionized to form a unique molecular ion, i.e., CH_2OH^+ (*m/z* 31), CH_2OD^+ (*m/z* 32), CD_2OH^+ (*m/z* 33), and CD_2OD^+ (*m/z* 34). When exposed to laser light between 460 and 510 nm or between 230 and 255 nm, hydroxymethyl cations produced no daughter ions.

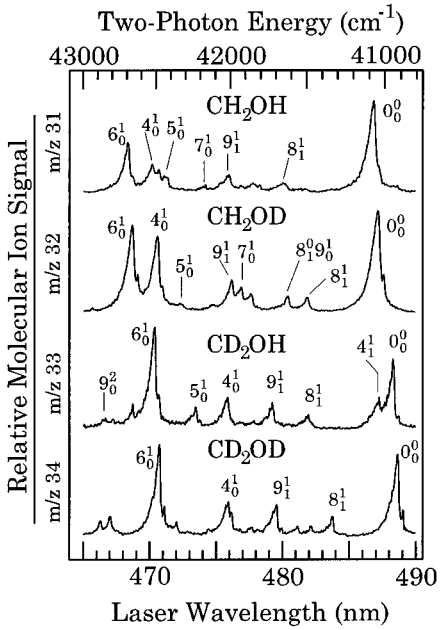

Figure 3. The 2+1 REMPI spectra of hydroxymethyl isotopomers between 465 and 490 nm.

To obtain maximum CH_2OH signal and to elevate the vibrational temperature, the reactor was operated with an excess of fluorine. Under these conditions numerous secondary reaction products are produced, including HCO,[147] CF,[148,149] HCF,[150] and CH_2F.[148] Over this study's spectral range these radicals did not exhibit interfering spectra.

Tables 9−12 list the REMPI bands observed during this study and their assignments. Figure 3 shows the 2+1 REMPI spectra of isotopomers of the hydroxymethyl radical between 465 and

TABLE 10: Band Maxima Observed in the 2+1 (2+2) REMPI and 1+1 REMPI (*m/z* 32) Spectra of CH_2OD Radicals[135]

λ_{air}, nm	$2h\nu_{obs}$, cm^{-1}	$2h(\nu_{obs}-\nu_o)$, cm^{-1}	λ_{air}, nm	$1h\nu_{obs}$, cm^{-1}	$1h(\nu_{obs}-\nu_o)$, cm^{-1}	assignment
501.63	39 859	−1185	250.80	39 860	−1170	6_1^0
497.65	40 178	−866	248.87	40 169	−861	7_1^0
496.86	40 242	−802	248.52	40 226	−804	8_2^0
494.26	40 453	−591				
493.76	40 494	−550	246.97	40 479	−551	9_2^0
491.42	40 687	−357	245.63	40 700	−330	8_3^1
489.96	40 808	−236	245.02	40 801	−229	$6_1^0 9_1^1$
			244.31	40 920	−110	$(6_1^1 9_2^0)^a$
487.14	41 044	0	243.65	41 030	0	0_0^0
481.84	41 496	452				8_1^1, (6_1^1),[b] $(4_0^1 6_1^0)^b$
480.39	41 621	577				$8_0^1 9_1^0$
477.61	41 863	819				$6_0^1 8_2^0$, $8_1^0 9_0^1$
476.89	41 927	883				7_0^1
476.16	41 991	947				9_1^1
474.76	42 114	1070				$6_0^1 9_2^0$
472.24	42 339	1295				5_0^1
470.94	42 456	1412				4_0^1 band head
470.56	42 490	1446				4_0^1
469.08	42 624	1580				6_0^1 band head
468.67	42 662	1618				6_0^1
465.66	42 937	1893				$4_0^1 8_1^1$

[a] Tentative assignment. [b] Transition that may also contribute to the band.

TABLE 11: Band Maxima Observed in the 2+1 (2+2) REMPI and 1+1 REMPI (*m/z* 33) Spectra of CD_2OH Radicals[135]

λ_{air}, nm	$2h\nu_{obs}$, cm^{-1}	$2h(\nu_{obs} - \nu_o)$, cm^{-1}	λ_{air}, nm	$1h\nu_{obs}$, cm^{-1}	$1h(\nu_{obs} - \nu_0)$, cm^{-1}	assignment
503.18	39 736	−1214	251.60	39 734	−1202	6_1^0
500.72	39 931	−1019	250.44	39 917	−1019	4_1^0
497.18	40 216	−734	248.68	40 200	−736	8_2^0
495.48	40 354	−596	247.80	40 343	−593	$8_1^0 9_1^0$
494.67	40 419	−531	247.57	40 380	−556	
494.31	40 449	−501	248.70	40 438	−498	9_2^0
			246.34	40 582	−354	
491.25	40 701	−249				$4_1^0 9_1^1$
489.96	40 808	−142	244.99	40 806	−130	$8_2^1 9_1^0$
488.49	40 931	−19	244.71	40 852	−84	
488.26	40 950	0	244.21	40 936	0	0_0^0
487.23	41 037	87				4_1^1
481.93	41 488	538				8_1^1, $8_1^0 9_0^1$
480.47	41 614	664				$8_0^1 9_1^0$
479.22	41 723	773				9_1^1
478.77	41 762	812				$6_0^1 8_2^0$
477.83	41 844	894				7_0^1
476.97	41 920	970				$6_0^1 8_1^0 9_1^0$
475.86	42 018	1068				4_0^1, $(6_0^1 9_2^0)^a$
473.43	42 233	1283				5_0^1
470.66	42 481	1531				6_0^1 band head
470.38	42 507	1557				6_0^1
468.73	42 657	1706				
467.21	42 795	1845				
466.66	42 846	1896				$8_0^1 9_0^1$, $(6_1^2)^a$

[a] Transition that may also contribute to the band.

TABLE 12: Band Maxima Observed in the 2+1 (2+2) REMPI and 1+2 REMPI (*m/z* 34) Spectra of CD_2OD Radicals[135]

λ_{air}, nm	$2h\nu_{obs}$, cm^{-1}	$2h(\nu_{obs} - \nu_o)$, cm^{-1}	λ_{air}, nm	$1h\nu_{obs}$, cm^{-1}	$1h(\nu_{obs} - \nu_o)$, cm^{-1}	assignment
503.61	39 702	−1218	251.90	39 688	−1223	6_1^0
501.42	39 876	−1044				$(8_1^0 9_3^0)^a$
501.06	39 904	−1016	250.63	39 888	−1023	4_1^0
497.92	40 156	−764	249.04	40 142	−769	
496.07	40 306	−614	248.12	40 291	−620	8_2^0
495.17	40 379	−541	247.65	40 367	−544	$8_1^0 9_1^0$
494.02	40 473	−447	247.07	40 463	−448	9_2^0
491.54	40 677	−243	245.77	40 676	−235	$8_2^1 9_1^0$
488.62	40 920	0	244.36	40 911	0	0_0^0
483.77	41 330	410				8_1^1
482.08	41 475	555				$8_0^1 9_1^0$, $6_0^1 4_1^0$
481.13	41 557	637				$4_0^1 9_2^0$
479.55	41 695	775				9_1^1
477.67	41 858	938				$6_0^1 8_2^0$
475.92	42 013	1093				4_0^1, $6_0^1 9_2^0$
474.44	42 143	1223				
472.03	42 358	1438				
471.10	42 442	1522				6_0^1 band head
470.74	42 475	1555				6_0^1
467.06	42 809	1889				$4_0^1 9_1^1$
466.31	42 878	1958				$6_0^1 8_1^1$

[a] Tentative assignment.

490 nm. Previous 2+1 REMPI studies have established that the intense bands near 487 nm are origins of 3p Rydberg states which reside near 41 000 cm^{-1}.[3,6,7] The REMPI spectra also exhibit vibrational progressions of which the most prominent arises from the ν_6' CO-stretch vibration of the 3p Rydberg state. Dulcey and Hudgens have reported similar spectra between 430 and 490 nm.[3,6]

Figure 4 shows the two-photon resonant REMPI spectra of isotopically selected hydroxymethyl radicals between 485 and 510 nm. Figure 4 does not depict the origin bands because

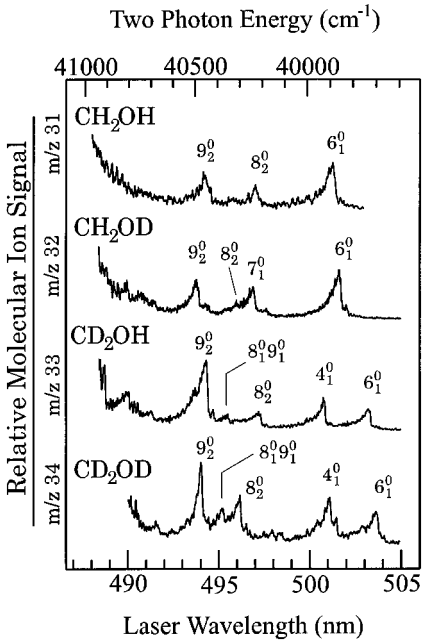

Figure 4. The 2+1 REMPI spectra of hydroxymethyl isotopomers between 485 and 510 nm that show the hot bands that originate from vibrationally populated levels of ground state radicals.

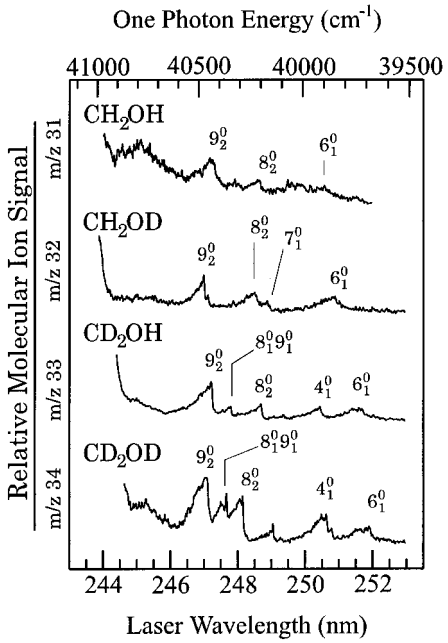

Figure 5. The 1+1 REMPI spectra of hydroxymethyl isotopomers between 244 and 254 nm that show the hot bands that originate from vibrationally populated levels of ground state radicals.

they are nearly 100 times more intense than the bands shown. These extremely weak bands are hot bands that arise from sparsely populated ground state vibrational levels. Besides their sparse populations, other factors conspire against the detection of hot bands by 2+1 REMPI spectroscopy. Because the ionization potential of CH_2OH is 7.56 eV,[5] hydroxymethyl radicals require four photons to ionize when $\lambda_{laser} > 492$ nm. Thus, most hot bands appear through a 2+2 REMPI mechanism. This 2+2 REMPI process may have a lower cross section than the 2+1 REMPI mechanism. Furthermore, the rotational envelopes of the origin bands of the 2+1 REMPI spectra extend for 100−200 cm^{-1} to each side of the band maximum. These widths complicate the identification of weak bands, particularly hot bands appearing near an origin band.

In an attempt to sidestep the problems incumbent with the 2+1 (2+2) REMPI spectra, we recorded 1+1 REMPI hot band spectra between 244 and 254 nm. These 1+1 REMPI spectra view the same vibrational levels as the 2+2 REMPI spectra; however, the REMPI mechanism remains constant. Unfortunately, the widths of the rotational envelopes are nearly the same as observed in the two-photon spectra. Figure 5 shows the corresponding one-photon resonant 1+1 REMPI spectra between 244 and 254 nm. In Tables 9−12 the one-photon and two-photon resonant spectra show corresponding transition energies. Each corresponding pair improves the confidence that the listed transition energy is a true absorption band of the hydroxymethyl radical.

Armed with the estimated vibrational frequencies (Tables 3−6), knowledge of the proper selection rules, and the Franck−Condon factors (Table 7), the REMPI spectra are interpreted directly. Each isotopomer's hot band spectrum (Figures 4 and 5) exhibits three clearly defined peaks, which we assign as the 6_1^0, 8_2^0, and 9_2^0 bands. CD_2OH and CD_2OD spectra also exhibit the $8_1^0 9_1^0$ combination band and the 4_1^0 fundamental band. To the blue of the origin bands, all isotopomer spectra also display 8_1^1 and 9_1^1 hot bands (Figure 3). Across these spectra hot band assignments are made involving ν_4'' and ν_6'' vibrational modes.

Table 13 summarizes the spectroscopic constants derived from the REMPI spectra. The symmetric (a′) fundamental vibrational frequencies of the ground and $\tilde{B}\ ^2A'(3p)$ Rydberg states are obtained directly from $\Delta v_n = \pm 1$ transitions. Because the REMPI data for unsymmetric ($\Delta v_8 + \Delta v_9 = 0, \pm 2, \pm 4, ...$) vibrations span an incomplete set of frequency relationships, we adopt infrared data and *ab initio* results to solve for the fundamental ν_8 torsion and ν_9 CH_2-wag frequencies. We obtain $1\nu_8'$ in $CH_2OH(\tilde{B}\ ^2A'(3p))$ by combining the 8_1^1 REMPI band with the $1^+ \leftarrow 0^+$ infrared band at 420 cm^{-1} (Table 6).[1] We obtain $1\nu_9''$ of $CH_2OH(\tilde{X}\ ^2A'')$ by combining the 9_1^1 REMPI band with the *ab initio* ν_9 CH_2-wag frequency of the cation. Since the REMPI spectra of CH_2OD, CD_2OH, and CD_2OD exhibit 8_1^1, 9_1^1, and $8_1^0 9_0^1$ bands, solutions for the ν_8 torsion ν_9 CH_2-wag frequencies require adoption of one *ab initio* frequency. In Table 13 the spectroscopic constants $1\nu_9''$, $1\nu_8''$, ν_8', and ν_9' are the average solutions obtained by substitutions with the *ab initio* ν_8' and ν_9' cation frequencies (Table 3). Each uncertainty reported for $1\nu_8''$, $1\nu_9''$, ν_8', and ν_9' in Table 13 includes the experimental uncertainty and the discord between the ν_8' and ν_9' substitution solutions.

Attempts to identify the $^2A'(4p)$ and $^2A'(5p)$ Rydberg states of isotopic hydroxymethyl radicals failed. The origin bands were expected to appear in 2+1 REMPI spectra near 390 and 362 nm, respectively, but with less intensity than exhibited by $\tilde{B}\ ^2A'(3p)$ Rydberg state. The inability to find these origins is disappointing because they would have enabled accurate spectroscopic determinations of adiabatic ionization potentials.

V. Thermochemical Properties of Hydroxymethyl Species

a. Heat Capacity Functions and Entropies. The heat capacities, $C_p°$, integrated heat capacities ($H_{298.15}° - H_T°$), and entropies, $S°$, of CH_2OH^+ and CH_2OH radical were calculated from their molecular partition functions using standard formulas. Table 14 lists the molecular structures, vibrational frequencies, and other parameters used to derive the molecular partition functions. Tables 15 and 16 list the thermochemical properties for CH_2OH^+ and CH_2OH, respectively. These values share the same reference states as adopted for the JANAF tables.[151] To keep Table 15 consistent with other thermodynamic tables,[151,152] the thermal electron convention is adopted for the calculation of thermodynamic properties for CH_2OH^+.[153]

TABLE 13: Spectroscopic Constants of Hydroxymethyl Radicals Derived from REMPI Spectra[135,144]

spectroscopic constant	CH_2OH	CH_2OD	CD_2OH	CD_2OD
		$\tilde{X}\ ^2A''$ State		
T_o, cm^{-1}	0	0	0	0
ν_4 (a′) CH_2 scissors, cm^{-1}			1019 ± 4	1020 ± 5
ν_6 (a′) CO stretch, cm^{-1}	1176 ± 7	1178 ± 11	1208 ± 10	1221 ± 4
ν_7 (a′) out-of-phase HCOH bend, cm^{-1}		864 ± 5		
$1\nu_8$ (a″) torsion, cm^{-1}		353 ± 9^b	347 ± 5^b	329 ± 23^b
$2\nu_8$ (a′) torsion, cm^{-1}	846 ± 6	803 ± 5	735 ± 4	617 ± 4
$3\nu_8$ (a″) torsion, cm^{-1}		1043 ± 15		
$1\nu_9$ (a″) CH_2 wag, cm^{-1}	234 ± 5^a	223 ± 9^b	221 ± 5^b	177 ± 23^b
$2\nu_9$ (a′) CH_2 wag, cm^{-1}	616 ± 6	550 ± 2	500 ± 4	448 ± 4
$\nu_8+\nu_9$ (a′), cm^{-1}			595 ± 4	543 ± 5
$\nu_9+2\nu_8$ (a″), cm^{-1}			1021 ± 10	962 ± 25
		$\tilde{B}\ ^2A'(3p)$ State		
T_o, cm^{-1}	41065 ± 3	41037 ± 10	40943 ± 10	40915 ± 5
ν_4 (a′) CH_2 scissors, cm^{-1}	1465 ± 7	1446 ± 7	1068 ± 7	1093 ± 7
ν_5 (a′) in-phase HCOH bend, cm^{-1}	1357 ± 7	1295 ± 7	1283 ± 7	
ν_6 (a′) CO stretch, cm^{-1}	1621 ± 7	1617 ± 7	1557 ± 7	1555 ± 7
ν_7 (a′) out-of-phase HCOH bend, cm^{-1}	1107 ± 7	882 ± 7	894 ± 7	
ν_8 (a″) torsion, cm^{-1}	993 ± 8^c	800 ± 7^b	885 ± 7^b	723 ± 23^b
ν_9 (a″) CH_2 wag, cm^{-1}	$(1175)^d$	1170 ± 7^b	994 ± 7^b	952 ± 23^b

[a] Derived using the *ab initio* ν_9 frequency of the cation. [b] Average of solutions obtained using *ab initio* ν_8 and ν_9 frequencies of the cation. See text. [c] Derived using $1\nu_8 = 420$ cm^{-1} from ref 1. [d] *Ab initio* ν_9 frequency of the cation.

TABLE 14: Physical Properties of the $^{12}CH_2{}^{16}OH$ Radical and Cation Used To Derive Thermodynamic Values

physical property	CH_2OH radical	CH_2OH cation
electronic state	$\tilde{X}\ ^2A''$	$\tilde{X}\ ^1A'$
internal rotational symmetry number, σ_i	2	2
ground state degeneracy	2	1
$I_aI_bI_c \times 10^{-120}$, $g^3\ cm^6$	3840.01[a]	2904.98[a]
ν_1 OH str, cm^{-1}	3650[b]	3423[c]
ν_2 CH_2 asym str, cm^{-1}	3159[a]	3214[a]
ν_3 CH_2 sym str, cm^{-1}	3019[a]	3068[a]
ν_4 CH_2 scissors, cm^{-1}	1459[b]	1465[d]
ν_5 in-phase HCOH bend, cm^{-1}	1334[b]	1357[d]
ν_7 CO str, cm^{-1}	1174[d]	1621[d]
ν_7 out-of-phase HCOH bend, cm^{-1}	1048[b]	1107[d]
$E_v(\nu_8,\nu_9)$ CH_2 wag and torsion manifold, cm^{-1}	0, 0.001, (234, 234),[d] (420, 420),[b] (616, 616),[d] 733.82, 734.28, (846, 846),[d] 975.6, 978.0, 1083.4, 1089.3, 1201.3, 1205.5, 1294, 1326, 1361.2, 1361.8, 1400, 1431, 1512, 1556, 1570, 1653, 1685, 1730, 1750, 1751, 1762, 1897, 1910, 1925, 1940, 1942, 1987, 2022, 2099, 2114, 2134, 2165, 2202, 2266, 2346, 2356, 2359, 2364, 2440, 2472, 2480, 2499, 2502, 2609, 2663, 2683, 2683, 2745, 2746, 2761, 2766, 2791, 2850, 2881, 2896, 3002, 3014, 3038, 3049, 3058, 3114, 3135, 3186.5, 3187, 3191, 3218, 3219, 3276, 3309, 3314, 3422, 3452, 3454, 3475, 3485, 3490, 3567, 3600, 3657, 3670, 3671, 3671, 3708, 3779, 3781, 3823, 3833, 3844, 3916, 3942, 3952, 4070, 4072, 4089, 4099, 4145, 4189.9, 4190.1, 4200, 4215, 4247, 4292, 4293, 4332, 4332, 4422, 4430, 4449, 4467, 4483, 4533, 4533, 4554, 4616, 4618, 4677, 4704, 4705, 4745, 4745, 4773, 4797, 4807, 4833, 4834, 4855, 4914, 4962.95, 4963.13, 4976, 4987, 4989, 5066, 5127, 5128, 5194, 5246, 5257, 5290, 5307, 5326, ..., {684 more levels}, ..., 29407[e]	0, 2×10^{-9}, (993, 993),[d] 1175.4, 1175.4, (1986, 1986),[f] 2151.3, 2151.3, 2344.2, 2344.2, 2881.4, 2881.4, 3111.4, 3111.4, 3317.9, 3317.9, 3505.4, 3505.4, 3802.1, 3802.1, 4053.4, 4053.4, 4276.2, 4276.2, 4476.1, 4476.1, 4658.5, 4658.5, 4696.8, 4696.8, 4974.4, 4974.4, 5217.1, 5217.1, 5432, 5432, 5557, 5557, 5625, 5625, 5802, 5802, 5870, 5870, 6138, 6138, 6371, 6371, 6380, 6380, 6380, 6578, 6578, 6733, 6734, 6764, 6764, 6936, 6936, 7034, 7034, 7117, 7123, 7291, 7291, 7514, 7514, 7552, 7555, 7698, 7712, 7712, 7785, 7891, 7891, ..., {372 more levels}, ..., 19916[e]
IP_a, eV	7.562 ± 0.004[g]	

[a] Calculated from the *ab initio* results (Tables 1, 3, and 5). [b] Experimental frequency from ref 1. [c] Experimental frequency from ref 19. [d] Experimental frequency of this work (Table 13). [e] Unmarked energy levels were calculated from the coupled CH_2-wag torsion potential energy surface. See text. [f] Estimated value of $2\nu_8$ based upon the experimental $1\nu_8$ (Table 13). [g] Derived from measurements of refs 5, 17, 18, 31, and 42. See text.

The moments of insertia used to calculate the rotational partition functions are based upon the *ab initio* structures optimized at the MP2/6-311G(2df,2p) level of theory (Table 1). For each species we weighted the translational and rotational contributions to $C°_p$, $(H°_{298.15} - H°_T)$, and $S°$, by the isotopic distributions of carbon, oxygen, and hydrogen.[154] Entropies of the radical include the usual entropy contribution by the electron spin degeneracy. The hydroxymethyl cation and radical also have an internal rotation that rapidly transforms their structures between two indistinguishable configurations, and we are counting all internal rotational states associated with this transformation; therefore, the internal rotation symmetry number, $\sigma_i = 2$, is used when estimating the rotational entropy contribution.[155,156]

An alternate way to deduce the appropriate symmetry number is by treating CH_2OH species with permutation−inversion group

TABLE 15: Thermochemical Properties of the CH_2OH Cation in JANAF Format at the Reference Pressure of 0.1 Mbar

T, K	C_p,[a] J (mol K)$^{-1}$	$S°$,[b] J (mol K)$^{-1}$	$-[G° - H(T_r)]/T$, J (mol K)$^{-1}$	$H°_{295.15} - H°_T$,[c] kJ mol^{-1}	$\Delta_f H°_T$, kJ mol^{-1}	$\Delta_f G°_T$, kJ mol^{-1}	log K_f
0	0	0		−10.149[d]	718.133	718.133	
100	33.259	190.723	259.113	−6.839			
200	33.967	213.879	231.354	−3.495			
250	35.502	221.605	228.657	−1.763			
298.15	37.835	228.047	228.047	0	716.386	732.876	−128.409
300	37.939	228.281	228.048	0.070	716.372	732.979	−127.635
350	40.996	234.354	228.520	2.042	716.001	735.777	−109.819
400	44.364	240.046	229.609	4.175	715.688	738.624	−96.463
450	47.808	245.470	231.072	6.479	715.453	741.504	−86.080
500	51.182	250.683	232.773	8.955	715.307	744.410	−77.775
600	57.470	260.582	236.594	14.393	715.272	750.238	−65.320
700	63.043	269.869	240.690	20.425	715.575	756.047	−56.422
800	67.951	278.615	244.890	26.980	716.190	761.788	−49.744
900	72.278	286.874	249.101	33.996	717.086	767.437	−44.545
1000	76.098	294.692	253.273	41.419	718.228	772.973	−40.380
1100	79.475	302.107	257.378	49.202	719.582	778.383	−36.966
1200	82.463	309.153	261.401	57.302	721.118	783.662	−34.115
1300	85.112	315.861	265.335	65.684	722.806	788.806	−31.698
1400	87.463	322.257	269.175	74.315	724.624	793.817	−29.620
1500	89.554	328.364	272.919	83.168	726.549	798.693	−27.816
1600	91.417	334.205	276.568	92.219	728.563	803.435	−26.232
1700	93.079	339.798	280.124	101.445	730.649	808.048	−24.831
1800	94.562	345.161	283.589	110.829	732.795	812.542	−23.582
1900	95.885	350.311	286.967	120.353	734.991	816.911	−22.461
2000	97.065	355.260	290.259	130.002	737.224	821.166	−21.449

[a] At all T the uncertainty is $|1\sigma| \leq 0.038$ J (mol K)$^{-1}$ and at 298.15 K, $\sigma = \pm 0.034$ J (mol K)$^{-1}$. [b] At all T the uncertainty is $|1\sigma| \leq 0.026$ J (mol K)$^{-1}$ and at 298.15 K, $\sigma = \pm 0.013$ J (mol K)$^{-1}$. [c] At all T the uncertainty is $|1\sigma| \leq 0.025$ kJ mol^{-1}. [d] Uncertainty $(1\sigma) = \pm 0.003$ kJ mol^{-1}.

TABLE 16: Thermochemical Properties of the CH_2OH Radical in JANAF Format at the Reference Pressure of 0.1 Mbar

T, K	C_p,[a] J (mol K)$^{-1}$	$S°$,[b] J (mol K)$^{-1}$	$-[G° - H°(T_r)]/T$, J (mol K)$^{-1}$	$H°_{298.15} - H°_T$, kJ mol^{-1}	$\Delta_f H°_T$, kJ mol^{-1}	$\Delta_f G°_T$, kJ mol^{-1}	log K_f
0	0	0		−11.781[d]	−11.488	−11.488	
100	37.074	199.004	282.664	−8.366	−14.084	−10.114	5.284
200	42.183	226.401	248.326	−4.385	−15.925	−5.417	1.415
250	44.658	236.074	244.934	−2.215	−16.874	−2.680	0.560
298.15	47.401	244.170	244.170	0	−17.800	0.138	−0.024
300	47.512	244.464	244.171	0.088	−17.835	0.250	−0.043
350	50.591	252.018	244.761	2.540	−18.766	3.338	−0.498
400	53.681	258.977	246.109	5.147	−19.643	6.555	−0.856
450	56.628	265.472	247.903	7.906	−20.463	9.879	−1.147
500	59.356	271.582	249.970	10.806	−21.224	13.292	−1.389
600	64.113	282.839	254.527	16.987	−22.595	20.326	−1.770
700	68.082	293.030	259.313	23.602	−23.787	27.576	−2.058
800	71.474	302.348	264.118	30.548	−24.824	34.985	−2.284
900	74.437	310.942	268.850	37.883	−25.723	42.515	−2.468
1000	77.058	318.924	273.464	45.460	−26.507	50.140	−2.619
1100	79.387	326.380	277.939	53.285	−27.189	57.838	−2.747
1200	81.458	333.379	282.272	61.329	−27.787	65.593	−2.855
1300	83.298	339.974	286.459	69.569	−28.319	73.397	−2.949
1400	84.929	346.208	290.507	77.982	−28.799	81.241	−3.031
1500	86.375	352.118	294.419	86.548	−29.239	89.115	−3.104
1600	87.654	357.735	298.203	95.251	−29.651	97.017	−3.168
1700	88.787	363.084	301.864	104.074	−30.048	104.943	−3.225
1800	89.789	368.188	305.408	113.004	−30.433	112.897	−3.277
1900	90.677	373.067	308.842	122.028	−30.816	120.870	−3.323
2000	91.464	377.739	312.171	131.136	−31.203	128.863	−3.366

[a] At all T the uncertainty is $|1\sigma| \leq 0.094$ J (mol K)$^{-1}$ and at 298.15 K, $\sigma = \pm 0.082$ J (mol K)$^{-1}$. [b] At all T the uncertainty is $|1\sigma| \leq 0.073$ J (mol K)$^{-1}$ and at 298.15 K, $\sigma = \pm 0.018$ J (mol K)$^{-1}$. [c] At all T the uncertainty is $|1\sigma| \leq 0.012$ kJ mol^{-1}. [d] Uncertainty $(1\sigma) = \pm 0.007$ kJ mol^{-1}.

theory.[157] Permutation−inversion group theory is particularly useful for nonrigid molecules because it considers internal rotation implicitly. CH_2OH species are members of the permutation−inversion group G_4. The symmetry number of G_4 members is $\sigma = 2$.

To compute the vibrational partition functions of the harmonic modes ν_1 through ν_7, we adopted experimentally observed frequencies, when known, and *ab initio* frequencies otherwise. For the cation we expanded the set of experimental vibrational frequencies by adopting the ν_4 CH_2 scissors and ν_7 out-of-phase HCOH bend frequencies of the $\tilde{B}\ ^2A'(3p)$ Rydberg state. We calculated the partition functions of the ν_8 torsion and ν_9 CH_2-wag modes by explicitly summing over their energy levels, $E_v(\nu_8,\nu_9)$, derived from the *ab initio* two-dimensional potential energy surfaces described above (Figure 2). The partition function for the CH_2OH radical includes 837 energy levels up to $E_v(\nu_8,\nu_9) = 29\,407$ cm^{-1}. The partition function for the CH_2OH cation includes 438 energy levels up $E_v(\nu_8,\nu_9) = 19\,856$ cm^{-1}. As indicated in Table 14, we have replaced certain $E_v(\nu_8,\nu_9)$ eigenvalues of the radical and cation with corresponding experimental energies obtained from the 2+1 and 1+1 REMPI spectra of $^{12}CH_2{}^{16}OH$ (Table 13).

Because the hydroxymethyl cation has a relatively large barrier ($B_\tau = 8331$ cm^{-1}) to internal rotation, we were able to verify our thermodynamic derivations by treating the hindered internal rotor as a harmonic vibration. In this picture the barrier to internal rotation is infinite, the parity levels vanish, and the cation has only one unique configuration; thus, the internal rotation symmetry number becomes $\sigma_i = 1$. For these computations we replace the list of $E_v(\nu_8,\nu_9)_{CH2OH+}$ (Table 14) with the harmonic frequencies $\nu_8 = 978$ cm^{-1} and $\nu_9 = 1175$ cm^{-1} (Table 3). Between 0 and 900 K this computational method yields essentially identical thermochemical values for $C°_p(CH_2OH^+)$, $(H°_{298.15} - H°_T)_{CH2OH+}$, and $S°(CH_2OH^+)$ as those obtained by explicit calculations from $E_v(\nu_8,\nu_9)_{CH2OH+}$. At higher temperatures ($T > 900$ K) the thermochemical values computed by the two methods diverge slightly. These divergences occur because the partition function computed from the list of $E_v(\nu_8,\nu_9)_{CH2OH+}$ levels (when $\sigma_i = 2$) contains information regarding the anharmonicity of the ν_8 and ν_9 energy levels.

b. The Adiabatic Ionization Potential of the CH_2OH Radical. The adiabatic ionization potential of CH_2OH is a spectroscopic quantity corresponding to the energy between the vibrationless radical and vibrationless cation. In practice, the most accurate IP_as are determined from extrapolations of the 0_0^0 bands of Rydberg series[128,158] and from zero kinetic energy electron (ZEKE) spectra.[159] No such determinations are available for hydroxymethyl radicals. Instead, the available IP_a determinations have involved photoionization spectra of thermal radicals.

Using vacuum ultraviolet (VUV) photoionization spectroscopy, Berkowitz, Klemm, and Dyke have measured ionization thresholds of thermalized CH_2OH and its isotopomers. Dyke et al.[5,42,131] observed the photoelectron spectrum and reported $IP_a(CH_2OH) = 7.56 \pm 0.01$ eV, $IP_a(CH_2OD) = 7.55 \pm 0.01$ eV, $IP_a(CD_2OH) = 7.55 \pm 0.01$ eV, and $IP_a(CD_2OD) = 7.56 \pm 0.01$ eV. Using VUV photoionization mass spectrometry, Ruscic and Berkowitz[31] have reported $IP_a(CD_2OH) = 7.540 \pm 0.006$ eV, and Klemm's laboratory[17,18] has reported $IP_a(CH_2OH) = 7.56 \pm 0.02$ eV, $IP_a(CH_2OD) = 7.55 \pm 0.02$ eV, $IP_a(CD_2OH) = 7.54 \pm 0.02$ eV,[17] and $IP_a(CD_2OD) = 7.53 \pm 0.02$ eV. Although these ionization thresholds are presumed to signify the energies of the 0_0^0 photoelectron bands, these spectra are not assigned with precision sufficient to assure that hot bands have not distorted one or more of the thresholds. The accuracy of $IP_a(CH_2OH)$ is improved by averaging. We can augment the data by adding the IP_as of deuterated isotopomers that are corrected for the difference in zero-point energies (ZPE) relative to CH_2OH. The *ab initio* results and the REMPI data provide two independent procedures for obtaining these corrections.

Simple differences among the *ab initio* ZPE (Tables 3 and 5) values can correct each isotopomer's IP_a to $IP_a(CH_2OH)$, e.g., $IP_a(CH_2OH) = IP_a(CD_2OD) - ZPE_{ion}(CD_2OD) + ZPE_{radical}(CD_2OD) + ZPE_{ion}(CH_2OH) - ZPE_{radical}(CH_2OH))$. Using the measurements given above, the ZPE corrections lead to nine independent values of $IP_a(CH_2OH)$. The average of these values, weighted by their reported deviations,[160] is $IP_a(CH_2OH) = 7.562 \pm 0.004$ eV.[139] Dyke's value of $IP_a(CD_2OD)$ is inconsistent with the data set and is discarded.

The REMPI data provide a second procedure for finding $IP_a(CH_2OH)$ from the isotopomers. Because the quantum defect of a Rydberg state is essentially invariant to isotopic substitution, the isotopic shifts of the 0_0^0 bands in the REMPI spectra are direct measurements of the correction factors, e.g., $IP_a(CH_2OH) = IP_a(CD_2OD) + T_o(CH_2OH) - T_o(CD_2OD)$. A weighted average (including the accuracy of each T_o) of the eight IP_a measurements from above gives $IP_a(CH_2OH) = 7.562 \pm 0.004$ eV, identical to the IP_a obtained from the *ab initio* ZPEs.

In summary, we recommend $IP_a(CH_2OH) = 7.562 \pm 0.004$ eV. We note that the weighted average of the five measurements from Klemm's[17,18] and Berkowitz's[31] laboratories gives the slightly more precise value, $IP_a(CH_2OH) = 7.560 \pm 0.001$ eV.

c. Enthalpy of Formation of the CH_2OH Cation and Radical. The appearance energy of CH_2OH^+ from CH_3OH provides estimates of the enthalpy of formation of the cation. VUV photoionization studies by Refaey and Chupka obtained $AP_0(CH_2OH^+/CH_3OH) = 11.67 \pm 0.03$ eV;[43] Ruscic and Berkowitz obtained $AP_0(CH_2OH^+/CH_3OH) = 11.649 \pm 0.003$ eV[92] and also extrapolated the 298 K appearance energy of Traeger and Holmes[90] to obtain $AP_0(CH_2OH^+/CH_3OH) = 11.632 \pm 0.007$ eV.[161] The average of these appearance potentials is $AP_0(CH_2OH^+/CH_3OH) = 11.650 \pm 0.019$ eV. From this average $AP_0(CH_2OH^+/CH_3OH)$, we compute $\Delta_f H°_0(CH_2OH^+) = AP_0(CH_2OH^+/CH_3OH) + \Delta_f H°_0(CH_3OH) - \Delta_f H°_0(H) - \Delta_f H°_0(e^-) = 718.1 \pm 1.8$ kJ mol^{-1}.[162,163] When combined with the heat correction (Table 16), we obtain $\Delta_f H°_{298.15}(CH_2OH^+) = 716.3 \pm 1.8$ kJ mol^{-1}.

The heats of formation for the CH_2OH radical and cation are related through the equation

$$\Delta_f H°_0(CH_2OH^+) = \Delta_f H°_0(CH_2OH) + IP_a(CH_2OH) \quad (5)$$

Using the adiabatic ionization potential derived above, we obtain $\Delta_f H°_0(CH_2OH) = -11.6 \pm 1.9$ kJ mol^{-1}. When combined with the heat correction (Table 16), the appearance energy data give $\Delta_f H°_{298.15}(CH_2OH) = -17.9 \pm 1.9$ kJ mol^{-1}.

Several groups have proposed values of $\Delta_f H°_{298}(CH_2OH)$ based upon the kinetic equilibria of the reactions

$$Cl + CH_3OH \underset{k_R}{\overset{k_f}{\rightleftharpoons}} HCl + CH_2OH \quad (6)$$

$$Br + CH_3OH \underset{k_R}{\overset{k_f}{\rightleftharpoons}} HBr + CH_2OH \quad (7)$$

$$I + CH_3OH \underset{k_R}{\overset{k_f}{\rightleftharpoons}} HI + CH_2OH \quad (8)$$

The "third-law" method obtains enthalpies of formation for the hydroxymethyl radical from the equilibrium constant of reactions 6−8 at specific temperatures. In this method, $K_{eq,T} = k_f/k_R$ is related to the Gibbs free energy of reactions 6−8 and to the reaction enthalpy through the equations

$$\Delta_r G_T = -RT \ln(K_{eq,T}) \quad (9)$$

$$\Delta_r H_T = T\Delta S_{r,T} + \Delta_r G_T \quad (10)$$

From the determinations of k_f and k_R, ΔG is obtained. Knowledge of entropies and heat capacities of all reactants, and products and the enthalpies of CH_3OH, HBr, and Br, allows calculation of $\Delta_f H°_{298.15}(CH_2OH)$.[162] In the following we use the entropy and heat capacities obtained during this study for these evaluations. Using the 298 K data for equilibrium of reaction 6 from the 1993 study by Dóbé et al.,[47] we obtain the third-law value, $\Delta_f H°_{298.15}(CH_2OH) = -13 \pm 5$ kJ mol^{-1}. Recently, Dóbé et al.[78] directly measured the forward and reverse rates of reaction 7, which enables a third-law determination (at 450 K) of $\Delta_f H°_{298.15}(CH_2OH) = -18.7 \pm 2.1$ kJ mol^{-1}. The forward rate data for reaction 8 by Cruickshank and Benson[79] and the reverse rate data by Seetula and Gutman,[50] evaluated at 586 K, give $\Delta_f H°_{298.15}(CH_2OH) = -13 \pm 8$ kJ

TABLE 17: Comparison of Bond Dissociation Energies,[144] D_0 (kJ mol^{-1}) and D_{298} (kJ mol^{-1}), of Various Species Containing the Hydroxymethyl Radical or Cation (Unless Noted Otherwise, Heats of Formation Are Derived from Ref 162)

bond	D_0, kJ mol^{-1}	D_{298}, kJ mol^{-1}	bond	D_0, kJ mol^{-1}	D_{298}, kJ mol^{-1}
H−CH_2OH^+	77.9 ± 1.9	89.1 ± 1.9	H−CH_2OH	394.3 ± 1.4	401.1 ± 1.4
CH_3−CH_2OH^+ [a]	74.0 ± 2.0	86.7 ± 2.0	CH_3−CH_2OH	374.6 ± 1.1	362.8 ± 1.6
OH−CH_2^+ [b]	709.8 ± 4.7	709.6 ± 4.7	CH_2−OH	436.6 ± 4.6	443.7 ± 4.6
CH_2O−H^+ [c]	705.2 ± 1.9	711.3 ± 1.9	CH_2O−H	123.1 ± 1.4	127.2 ± 1.4

[a] Values of $\Delta_f H°_T(CH_3CH_2OH^+)$ are from ref 44. [b] Values of $\Delta_f H°_T(CH_2^+)$ are from ref 44. [c] Values of $\Delta_f H°_T(CH_2O^+)$ are from ref 44.

mol^{-1}. The weighted average of these three determinations is $\Delta_f H°_{298.15}(CH_2OH) = -17.6 \pm 1.9$ kJ mol^{-1}.

The shock tube study by Tsang[83] also obtained the heat of formation of CH_2OH. By comparing the relative stability of CH_3OH with CH_4 and referencing these data to the CH_3−H bond strength, Tsang estimated that $\Delta_f H°_{298}(CH_2OH) = -17.6 \pm 8$ kJ mol^{-1}. Unlike the photoionization appearance energy and kinetic equilibrium methods, this estimate does not rely upon prior knowledge of reactant entropies and heat capacities.

The weighted average of the enthalpies of formations derived from the appearance potentials, the kinetic equilibria, and shock tube results yields our recommended value, $\Delta_f H°_{298.15}(CH_2OH) = -17.8 \pm 1.3$ kJ mol^{-1}. We also recommend $\Delta_f H°_0(CH_2OH) = -11.5 \pm 1.3$ kJ mol^{-1}, $\Delta_f H°_0(CH_2OH^+) = 718.1 \pm 1.8$ J mol^{-1}, and $\Delta_f H°_{298.15}(CH_2OH^+) = 716.4 \pm 1.8$ kJ mol^{-1}.

Table 17 lists bond dissociation energies, D_0 and D_{298}, for compounds containing CH_2OH^+ and CH_2OH. From the heats of formation of the ion we can also calculate the proton affinity of formaldehyde. We obtain $PA_0(CH_2O) = 705.2 \pm 1.9$ kJ mol^{-1} and $PA_{298}(CH_2O) = 711.3 \pm 1.9$ kJ mol^{-1}.[162]

VI. Discussion

a. Spectroscopic and *ab Initio* Results. Perhaps the most surprising discovery of this work is that hydroxymethyl radicals belong to the C_s point group and the G_4 permutation−inversion group. This higher symmetry alters interpretations of the spectroscopic data and estimations of thermochemical properties of the hydroxymethyl radical and cation. In previous reports the vibrational assignment schemes of $\tilde{B}\ ^2A'(3p) \leftarrow \tilde{X}\ ^2A''$ REMPI spectra were performed with the assumption that hydroxymethyl radicals are totally unsymmetric and belong to the C_1 point group. If the CH_2OH radical were unsymmetric, all fundamental vibrational frequencies of the upper and lower electronic states could be determined by direct observation of N_0^1 and N_1^0 bands (where $N = 1-9$). However, because ground and Rydberg radicals belong to the C_s point group, the 8_0^1 and 9_0^1 bands are forbidden. Thus, previous assignments[6] of 8_0^1 and 9_0^1 bands in the REMPI spectra of hydroxymethyl radicals are incorrect and are reassigned in this work as 8_1^1 and 9_1^1 bands, respectively. In this work we reassign the previous assignments by Bomse et al.[7] of 8_1^0 and 9_1^0 hot bands in the REMPI spectra of CH_2OH and CD_2OH as the 8_2^0 and 9_2^0 bands, respectively. These reassignments change the vibrational frequencies derived for the ν_8 through ν_9 modes of the ground and $\tilde{B}\ ^2A'(3p)$ Rydberg states (Table 13).

The spectroscopic data and *ab initio* results presented here firmly establish that the hydroxymethyl radical contains a hindered rotor possessing 2-fold symmetry and a barrier $B_\tau = 1643$ cm^{-1}. This barrier agrees closely with 1600 cm^{-1} activation energy to internal rotation inferred from temperature dependent ESR data[33] and a previous high level calculation.[89] Our *ab initio* calculations and spectral data also indicate that a small barrier, $B_{wag} = 156$ cm^{-1}, stabilizes the pyramidal geometry at the carbon center.

This study has demonstrated that the torsion and CH_2-wag motions of hydroxymethyl species are mixed modes. The cations exhibit weak mixing for the spectroscopically important vibrational levels. Our computer model predicts that mixing in the cations becomes strong as the high torsion barrier is approached. Because the cations have weak vibrational couplings, the experimentally observed isotopic ν_8 and ν_9 frequencies (Table 13) conform to those predicted from the frequencies of CH_2OH^+ by the (uncoupled) harmonic oscillator relationships

$$\nu_8^i = \nu_8^{CH2OH}\sqrt{\frac{I_{torsion}^{CH2OH}}{I_{torsion}^i}} \tag{11}$$

and

$$\nu_9^i = \nu_9^{CH2OH}\sqrt{\frac{I_{wag}^{CH2OH}}{I_{wag}^i}} \tag{12}$$

where I_{wag} and $I_{torsion}$ are listed in Table 2. However, in the radical these isotopic relationships fail completely because the torsion and CH_2-wag motions are strongly coupled for all vibrational levels. Equation 11 does not even predict the proper direction of change for $2\nu_8$. For example, the $I_{torsion}$ of CH_2-OD to CD_2OH decreases from 0.882 to 0.695 amu Å^2. Using $2\nu_8^{CH2OH} = 846$ cm^{-1} (Table 13), eq 11 predicts a frequency *increase* from 678 to 764 cm^{-1}, respectively. In contrast, the experimental data exhibit a *decrease* from $2\nu_8^{CH2OD} = 803$ cm^{-1} to $2\nu_8^{CD2OH} = 735$ cm^{-1} (Tables 6 and 13). Our model of the two-dimensional potential energy surface correctly predicts the proper isotopic shifts and frequencies ($2\nu_8^{CH2OD} = 788$ cm^{-1} and $2\nu_8^{CD2OH} = 737$ cm^{-1}; Table 6) because it implicitly accounts for the contributions of the CH_2-wag and torsion motions. In summary, neither the ν_8 nor the ν_9 vibrational level of hydroxymethyl radicals is adequately predicted using the harmonic normal mode description. The amount of mixing (hence, the fractional contribution of I_{wag} and $I_{torsion}$) changes for each quantum level. These levels are properly predicted only by two-dimensional models of the potential energy surface.

Our results clarify the assignment of the 569 cm^{-1} band attributed to CH_2OH trapped in a cryogenic Ar matrix. In her 1981 paper Jacox reported that the 569 cm^{-1} band was observed when the sample matrix was prepared using the reaction F + CH_3OH. This band was absent when the sample matrix was prepared by the reacting metastable argon atoms with CH_3OH.[1] Jacox suggested that the 569 cm^{-1} band originated either from the ν_9 CH_2-wag mode of CH_2OH or from a CH_2OH·HF complex. Recently, Bauschlicher and Partridge concluded that the 569 cm^{-1} band originated from the ν_9 CH_2-wag mode of the CH_2OH radical.[100,135] Their conclusion was supported by the coincidence of this band with the (scaled) harmonic frequency obtained from MP2/6-311+G(3df,2p) calculations. However, because the ν_9 CH_2-wag mode of CH_2OH is not a harmonic oscillator, this frequency coincidence is fortuitous and their conclusion is inappropriate. Neither our *ab initio* calculations (Table 6) nor the REMPI spectrum (Table 9) supports assignment of this band to the CH_2OH radical. The fundamental frequency of the ν_9 CH_2-wag mode of CH_2OH is 235 cm^{-1}, and no vibrational levels of CH_2OH reside at 569 cm^{-1} (Tables

6 and 13). Therefore, the present negative evidence supports Jacox's hypothesis that the 569 cm^{-1} band originates from an absorption of a $CH_2OH{\cdot}HF$ complex.

b. Thermodynamic Derivations. In this study we recommend the value $\Delta_f H°_{298.15}(CH_2OH) = 17.8 \pm 1.3$ kJ mol^{-1} on the basis of ion appearance potentials, kinetic equilibria, and shock tube data. The *ab initio* results also support this value. Several authors[47,50,78,90,92] have reviewed previous determinations of $\Delta_f H°_{298}(CH_2OH)$. These determinations span $\Delta_f H°_{298}(CH_2OH) < -34$ to -8.9 kJ mol^{-1}.[47,50,78,81,90,92,98] As this study began, the preferred values of $\Delta_f H°_{298}(CH_2OH)$ had aligned into two groups: (1) determinations based upon the ion appearance potential, $AP_0(CH_2OH^+/CH_3OH)$, which had obtained values between -16.6 and -20.4 kJ mol^{-1} [18,90,92] and (2) determinations based upon kinetic equilibria of reactions 6−8, which had obtained values between -8.9 and -12 kJ mol^{-1}.[47,50,88] The 5−11 kJ mol^{-1} differences between the ion and kinetic determinations seemed irreconcilable.

This work's new thermochemical properties lower the "third-law" kinetic equilibrium determinations of $\Delta_f H°_{298.15}(CH_2OH)$ by 3−4 kJ mol^{-1}; for example, re-evaluations of earlier kinetic data for reactions 7−9 yield $\Delta_f H°_{298.15}(CH_2OH) \sim -13$ kJ mol^{-1}. Although these re-evaluations still disagree with the ion data, the discord is moderated by the large uncertainties manifested by these kinetic determinations (e.g., between ± 5 and ± 8 kJ mol^{-1}).

In the preceding paper Dóbé et al.[78] reported new kinetic rate data for reaction 7. Using excimer laser photolysis coupled with Br atom resonance fluorescence, they obtained the first direct measurement of the reaction rate of Br + CH_3OH. At 450 K this new reaction rate is about 10 times faster than the rate obtained from the previous photobromination study.[81] They also measured the reverse reaction, HBr + CH_2OH, using laser magnetic resonance to monitor the CH_2OH radicals in a flow reactor. The new equilibrium constant, K_{eq}, computed from these rates leads to the third-law value, $\Delta_f H°_{298.15}(CH_2OH) = -18.7 \pm 2.1$ kJ mol^{-1}. This value agrees with the ion and shock tube determinations, and its small uncertainty allows it to anchor our evaluation of $\Delta_f H°_{298.15}(CH_2OH)$.

The *ab initio* results also support this evaluation. During this study we obtained the theoretical value $\Delta_f H°_{298.15}(CH_2OH) = -18.4 \pm 1.3$ kJ mol^{-1} from CBS-QCI/APNO calculations that are corrected for nonharmonic vibrational ZPE contributions (Table 8). In an earlier study, Espinosa-García and Olivaries del Valle[91] reported a higher theoretical heat of formation, $\Delta_f H°_{298}(CH_2OH) = -15.6 \pm 1.5$ kJ mol^{-1}, based upon MP4 computations. Their thermocorrection for CH_2OH, TC(298 K) = 24.98 kcal mol^{-1}, is too high because it was derived using harmonic ν_8 torsion and ν_9 CH_2-wag frequencies. Using this work's ZPE and $(H°_{298.15} - H°_T)$, we obtain TC(298 K) = 24.46 kcal mol^{-1}. When this TC(298 K) is applied to their calculations, their MP4 theoretical heat of formation becomes $\Delta_f H°_{298}(CH_2OH) = -17.8 \pm 1.5$ kJ mol^{-1}. In summary, the theoretical and experimental values of $\Delta_f H°_{298.15}(CH_2OH)$ are in good agreement.

This paper and the preceding paper by Dóbé et al.[78] have thoroughly examined and evaluated the spectroscopy, potential energy surfaces, kinetics, and thermochemistry of hydroxymethyl radical species. Because our evaluation methods differ, we arrive at slightly different $\Delta_f H°_{298}(CH_2OH)$'s (i.e., -17.8 *vs* -16.6 kJ mol^{-1}). Dóbé et al. give weight to second-law evaluations of reaction 7 and adopt a lower literature value of $IP_a(CH_2OH)$; we use only third-law methods to evaluate reaction 7, and the analysis of photoionization data caused us to adopt a higher $IP_a(CH_2OH)$. Within their respective ± 1.3 kJ mol^{-1} error limits both evaluations of $\Delta_f H°_{298}(CH_2OH)$ agree.

Regardless of the evaluation protocol, the quality of the available data limits further refinements of $\Delta_f H°_{298}(CH_2OH)$. In particular, ion-based determinations need an $AP_0(CH_2OH^+/CH_3OH)$ that is better defined (extrapolated values from 298 K samples are inadequate) and an $IP_a(CH_2OH)$ of spectroscopic accuracy (i.e., an uncertainty smaller than ± 5 cm^{-1}). Determinations of $\Delta_f H°_{298}(CH_2OH)$ from kinetic equilibria need second law plots that extrapolate to known $S°_T(CH_2OH)$ (Table 16). The pre-exponent of reaction (−7), HBr + CH_2OH, needs further investigation. Dóbé et al.[78] report a preexponential value that is twice that reported by Seetula and Gutman.[50] The k_{-7} rates reported by Seetula and Gutman[50] from their laser flash photolysis studies would lower $\Delta_f H°_{298}(CH_2OH)$ slightly.

VII. Conclusion

This unified theoretical and experimental study has improved the understanding of the structure and vibrational energy manifolds of hydroxymethyl radicals and cations. The thermochemical properties derived from these results, particularly for $S°_{298.15}(CH_2OH)$, appear to resolve the discord that has existed between previous evaluations of $\Delta_f H°_{298.15}(CH_2OH)$ obtained from ion appearance potential measurements and from kinetic equilibrium measurements. Interpretations of the existent experimental data indicate that $\Delta_f H°_{298.15}(CH_2OH) = -17.8$ kJ mol^{-1}. *Ab initio* calculations also support this heat of formation.

Acknowledgment. This work was supported in part by the U.S.−Hungarian Science and Technology Program (JF ID No. 243/92a). We thank Dr. Tibor Bérces of the Hungarian Academy of Sciences for his comments, discussions, and data on the equilibrium of the Br + CH_3OH reaction prior to publication. We also thank Prof. Alan Rogers (Texas A&M University), Dr. Joseph Berkowitz (Argonne National Laboratory), and Dr. Karl K. Irikura (NIST) for thoughtful discussions.

References and Notes

(1) Jacox, M. E. *Chem. Phys.* **1981**, *59*, 213.
(2) Jacox, M. E.; Milligan, D. E. *J. Mol. Spectrosc.* **1973**, *47*, 148.
(3) Dulcey, C. S.; Hudgens, J. W. *J. Phys. Chem.* **1983**, *87*, 2296.
(4) Dulcey, C. S.; Hudgens, J. W. *Bull. Soc. Chim. Belg.* **1983**, *92*, 583.
(5) Dyke, J. M.; Ellis, A. R.; Jonathan, N.; Keddar, N.; Morris, A. *Chem. Phys. Lett.* **1984**, *111*, 207.
(6) Dulcey, C. S.; Hudgens, J. W. *J. Chem. Phys.* **1986**, *84*, 5262.
(7) Bomse, D. S.; Dougal, S.; Woodin, R. L. *J. Phys. Chem.* **1986**, *90*, 2640.
(8) Tyndall, G. S.; Wallington, T. J.; Hurley, M. D.; Schneider, W. F. *J. Phys. Chem.* **1993**, *97*, 1576.
(9) Heinemannfiedler, P.; Hoyermann, K. *Ber. Bunsen-Ges. Phys. Chem.* **1988**, *92*, 1472.
(10) Tortajada, J.; Audier, H. E.; Monteiro, C.; Mourgues, P. *Org. Mass Spectrosc.* **1991**, *26*, 913.
(11) Hvistendahl, G.; Uggerud, E. *Org. Mass Spectrosc.* **1991**, *26*, 67.
(12) Terlouw, J. K.; Holmes, J. L.; Burgers, P. C. *Int. J. Mass Ion Processess* **1985**, *66*, 239.
(13) Holmes, J. L.; Terlouw, J. K. *Org. Mass Spectrosc.* **1986**, *21*, 776.
(14) Davies, A. G.; Neville, A. G. *J. Chem. Soc., Perkin Trans. 2* **1991**, *1991*, 2021.
(15) Zha, Q. M.; Nishimura, T.; Bertrand, M. J.; Meisels, G. G. *Int. J. Mass Spectrom.* **1991**, *107*, 515.
(16) Mourgues, P.; Audier, H. E.; Leblanc, D.; Hammerum, S. *Org. Mass Spectrosc.* **1993**, *28*, 1098.
(17) Tao, W.; Klemm, R. B.; Nesbitt, F. L.; Stief, L. J. *J. Phys. Chem.* **1992**, *96*, 104.
(18) Kuo, S.-C.; Zhang, Z.; Klemm, R. B.; Liebman, J. F.; Stief, L. J.; Nesbitt, F. L. *J. Phys. Chem.* **1994**, *98*, 4026.
(19) Amano, T.; Warner, H. E. *Astrophys. J.* **1989**, *342*, L99.
(20) Pagsberg, P.; Munk, J.; Anastasi, C.; Simpson, V. J. *Chem. Phys. Lett.* **1989**, *157*, 171.
(21) Pagsberg, P.; Munk, J.; Anastasi, C.; Simpson, V. J. *Chem. Phys. Lett.* **1988**, *146*, 375.

(22) Botschwina, P. In *Ion and Cluster Ion Spectroscopy and Structure*; Maier, J. P., Ed.; Elsevier: Amsterdam, 1989; pp 93−94.
(23) Hudgens, J. W. In *Advances in Multiphoton Processes and Spectroscopy*; Lin, S. H., Ed.; World Scientific: Singapore, 1988; Vol. 4, pp 171−296.
(24) Sanders, N.; Butler, J. E.; Pasternack, L. R.; McDonald, J. R. *Chem. Phys.* **1980**, *48*, 203.
(25) Pople, S. A.; Hillier, I. H.; Guest, M. F.; Colburn, E. A.; Kendrixk. *Surf. Sci.* **1984**, *139*, 299.
(26) Dixon, W. T.; Norman, R. O. C. *J. Chem. Phys.* **1971**, *1963*, 3119.
(27) Dobbs, A. J.; Gilbert, B. C.; Norman, R. O. C. *J. Chem. Soc. A* **1971**, *1971*, 124.
(28) Livingston, R.; Zeldes, H. *J. Chem. Phys.* **1966**, *44*, 1245.
(29) Hoyermann, K.; Loftfield, N. S.; Sievert, R.; Wagner, H. G. *Symp.* (*Int.*) *Combust.* [*Proc.*] **1981**, *18*, 831.
(30) Pagsberg, P.; Munk, J.; Anastasi, C.; Simpson, V. *Chem. Phys. Lett.* **1989**, *157*, 271.
(31) Ruscic, B.; Berkowitz, J. *J. Chem. Phys.* **1991**, *95*, 4033.
(32) Hudson, A. *J. Chem. Soc. A* **1969**, 2513.
(33) Krusic, P. J.; Meakin, P.; Jesson, J. P. *J. Phys. Chem.* **1971**, *75*, 3438.
(34) Fessenden, R. W. *J. Phys. Chem.* **1967**, *71*, 74.
(35) Dixon, W. T.; Norman, R. O. C. *J. Chem. Soc.* **1963**, 3119.
(36) Fujimoto, M.; Ingram, D. J. E. *Trans. Faraday Soc.* **1958**, *54*, 1304.
(37) Gibson, J. F.; Symons, M. C. R.; Townsend, M. G. *J. Chem. Soc.* (*London*) **1959**, 269.
(38) Symons, M. C. R.; Townsend, M. G. *J. Chem. Soc.* (*London*) **1959**, 263.
(39) Symons, M. C. R. *J. Chem. Soc.* (*London*) **1959**, 277.
(40) Tortajada, J.; Audier, H. E.; Monteiro, C.; Mourgues, P. *Org. Mass Spectrosc.* **1991**, *26*, 913.
(41) Hudson, A.; Root, K. D. J. *Tetrahedron* **1969**, *25*, 5311.
(42) Dyke, J. M. *J. Chem. Soc., Faraday Trans. 2* **1987**, *83*, 69.
(43) Refaey, K. M. A.; Chupka, W. A. *J. Chem. Phys.* **1968**, *48*, 5205.
(44) Lias, S. G.; Liebman, J. F.; Levin, R. D. *J. Phys. Chem. Ref. Data* **1984**, *13*, 695.
(45) Holmes, J. L.; Lossing, F. P. *Int. J. Mass Spectrom. Ion Processes* **1984**, *58*, 113.
(46) Schlutter, J. S. R.; Kleinermanns, K. *Chem. Phys. Lett.* **1993**, *213*, 262.
(47) Dóbé, S.; Otting, M.; Temps, F.; Wagner, H. G.; Ziemer, H. *Ber. Bunsen-Ges. Phys. Chem.* **1993**, *97*, 877.
(48) Seetula, J. A.; Kalinovski, I. J.; Slagle, I. R.; Gutman, D. *Chem. Phys. Lett.* **1994**, *224*, 533.
(49) Getoff, N.; Ritter, A.; Schworer, F.; Bayer, P. *Radiat. Phys. Chem.* **1993**, *41*, 797.
(50) Seetula, J. A.; Gutman, D. *J. Phys. Chem.* **1992**, *96*, 5401.
(51) Pagsberg, P.; Munk, J.; Anastasi, C.; Simpson, V. J. *J. Phys. Chem.* **1989**, *93*, 5162.
(52) Grotheer, H. H.; Riekert, G.; Walter, D.; Just, T. *Chem. Phys. Lett.* **1988**, *148*, 530.
(53) Nesbitt, F. L.; Payne, W. A.; Stief, L. J. *J. Phys. Chem.* **1988**, *92*, 4030.
(54) Dóbé, S.; Temps, F.; Bohland, T.; Wagner, H. G. *Z. Naturforsch. A* **1985**, *40*, 1289.
(55) Grotheer, H. H.; Riekert, G.; Meier, U.; Just, T. *Ber. Bunsen-Ges. Phys. Chem.* **1985**, *89*, 187.
(56) Durant, J. L. *J. Phys. Chem.* **1991**, *95*, 10701.
(57) Nesbitt, F. L.; Payne, W. A.; Stief, L. J. *J. Phys. Chem.* **1989**, *93*, 5158.
(58) Shimizu, Y.; Sugimoto, S.; Kawanishi, S.; Suzuki, N. *Bull. Chem. Soc. Jpn.* **1991**, *64*, 3607.
(59) Tsang, W. *J. Phys. Chem. Ref. Data* **1987**, *16*, 471.
(60) Radford, H. E. *Chem. Phys. Lett.* **1980**, *71*, 195.
(61) Batt, L.; Burrows, J.; Robinson, G. N. *Chem. Phys. Lett.* **1981**, *78*, 467.
(62) Bogan, D.; Kaufman, M. J.; Hand, C. W.; Sanders, W. A.; Brauer, B. E. *J. Phys. Chem.* **1990**, *94*, 8128.
(63) Meier, U.; Grotheer, H. H.; Just, T. *Chem. Phys. Lett.* **1984**, *106*, 97.
(64) MacDonald, R. G.; Sloan, J. J.; Wassell, P. T. *Chem. Phys.* **1979**, *41*, 201.
(65) Grotheer, H. H.; Just, T. *Chem. Phys. Lett.* **1981**, *78*, 71.
(66) Niki, H.; Maker, P. D.; Savage, C. M.; Breitenbach, L. P. *J. Chem. Phys.* **1978**, *82*, 135.
(67) Aikin, A. C.; Herman, J. R.; Maier, E. J. *Proceedings of the NATO Advanced Study Institute on Atmospheric Ozone*; Dordrecht: Holland, 1979.
(68) Kerr, J. A. *Chem. Rev.* **1966**, *66*, 465.
(69) Seinfeld, J. H.; Allario, F.; Bandeen, W. R.; Chameides, W. L.; Davies, D. D.; Hinkley, E. D.; Steward, R. W. NASA Ref. Publ. No. 1062; 1981.
(70) Gray, P.; Williams, A. *Chem. Rev.* **1959**, *59*, 239.
(71) Gray, P.; Shaw, R.; Thyme, J. *J. Prog. React. Kinet.* **1967**, 63.
(72) Heicklen, J. *Atmospheric Chemistry*; Academic: New York, 1976.
(73) Leighton, P. *Photochemistry of Air Pollution*; Academic: New York, 1981.
(74) *Oxidation of Organic Compounds*; American Chemical Society: Washington, DC, 1968.
(75) Demerjian, K. L.; Kerr, J. A.; Calvert, J. A. *Adv. Environ. Sci. Technol.* **1974**, *4*, 1.
(76) Smith, D. J.; Setser, D. W.; Kim, K. C.; Bogan, D. J. *J. Phys. Chem.* **1977**, *81*, 898.
(77) Dill, B.; Heydtmann, H. *Chem. Phys.* **1980**, *54*, 9.
(78) Dóbé, S.; Bérces, T.; Turányi, T.; Márta, F.; Gussdorf, J.; Temps, F.; Wagner, H. G. *J. Phys. Chem.* **1996**, *100*, 19864.
(79) Cruickshank, F. R.; Benson, S. W. *J. Phys. Chem.* **1969**, *73*, 733.
(80) Seetula, J. A.; Gutman, D. *J. Phys. Chem.* **1991**, *95*, 3626.
(81) Buckley, E.; Whittle, E. *Trans. Faraday Soc.* **1962**, *58*, 536.
(82) Dóbé, S.; Bérces, T.; Temps, F.; Wagner, H. G.; Ziemer, H. *J. Phys. Chem.* **1994**, *98*, 9792.
(83) Tsang, W. *Int. J. Chem. Kinet.* **1976**, *8*, 173.
(84) Westbrook, C. K.; Dryer, F. L. *Combust. Sci. Technol.* **1979**, *20*, 125.
(85) Michael, J. V.; Nava, D. F.; Payne, W. A.; Steif, L. J. *J. Phys. Chem.* **1979**, *70*, 3652.
(86) Tsuboi, T.; Hashimoto, K. *Combust. Flame* **1981**, *42*, 61.
(87) Whitten, J. E.; Young, C. E.; Pellin, M. J.; Gruen, D. M.; Jones, P. L. *Surf. Sci.* **1991**, *241*, 73.
(88) Dóbé, S. *Z. Phys. Chem. Part 1* **1992**, *175*, 123.
(89) Bauschlicher, C. W., Jr.; Partridge, H. *J. Phys. Chem.* **1994**, *98*, 1826.
(90) Traeger, J. C.; Holmes, J. L. *J. Phys. Chem.* **1993**, *97*, 3453.
(91) Espinosa-García, J.; Olivares del Valle, F. J. *J. Phys. Chem.* **1993**, *97*, 3377.
(92) Ruscic, B.; Berkowitz, J. *J. Phys. Chem.* **1993**, *97*, 11451.
(93) Curtiss, L. A.; Kock, L. D.; Pople, J. A. *J. Chem. Phys.* **1991**, *95*, 4040.
(94) Burcat, A. Thermochemical Data for Combustion Calculations. In *Combustion Chemistry*; Gardiner, W. C., Jr., Ed.; Springer-Verlag: New York, 1984; pp 455−504.
(95) Haney, M. A.; Franklin, J. L. *Trans. Faraday Soc.* **1969**, *65*, 1794.
(96) Bauschlicher, C. W., Jr.; Langhoff, S. R.; Walch, S. P. *J. Chem. Phys.* **1992**, *96*, 450.
(97) Ma, N. L.; Smith, B. J.; Pople, J. A.; Radom, L. *J. Am. Chem. Soc.* **1991**, *113*, 7903.
(98) Golden, D. M.; Benson, S. W. *Chem. Rev.* **1969**, *69*, 125.
(99) McMillen, D. F.; Golden, D. M. *Annu. Rev. Phys. Chem.* **1982**, *33*, 493.
(100) Bauschlicher, C. W., Jr.; Partridge, H. *Chem. Phys. Lett.* **1993**, *215*, 451.
(101) Tachikawa, H. *Chem. Phys. Lett.* **1993**, *212*, 27.
(102) Walch, S. P. *J. Chem. Phys.* **1993**, *98*, 3076.
(103) Uggerud, E.; Helgaker, T. *J. Am. Chem. Soc.* **1992**, *114*, 4265.
(104) Kalkanis, G. H.; Shields, G. C. *J. Phys. Chem.* **1991**, *95*, 5085.
(105) Tachikawa, H.; Lunell, S.; Tornkvist, C.; Lund, A. *THEOCHEM* **1994**, *110*, 25.
(106) Solgadi, D.; Flament, J. P. *Chem. Phys.* **1985**, *98*, 387.
(107) Saebo, S.; Radom, L.; Schaefer, H. F. *J. Chem. Phys.* **1983**, *78*, 845.
(108) Adams, G. F.; Bartlett, R. J.; Purvis, G. D. *Chem. Phys. Lett.* **1982**, *87*, 311.
(109) Greenhill, P. G.; Ogrady, B. V.; Gilbert, R. G. *Austral. J. Chem.* **1986**, *39*, 1929.
(110) Rettrup, S.; Pagsberg, P.; Anastasi, C. *Chem. Phys.* **1988**, *122*, 45.
(111) Wong, M. W.; Pross, A.; Radom, L. *J. Am. Chem. Soc.* **1994**, *116*, 6284.
(112) Arakawa, R. *Bull. Chem. Soc. Jpn.* **1988**, *61*, 3425.
(113) Carpenter, J. E.; Weinhold, F. *THEOCHEM* **1988**, *46*, 41.
(114) DeFrees, D. J.; McLean, A. D. *J. Chem. Phys.* **1985**, *82*, 333.
(115) Ha, T. *Chem. Phys. Lett.* **1975**, *30*, 379.
(116) Bernadi, F.; Epiotis, N. D.; Cherry, W.; Schlegel, H. B.; Whangbo, M. H.; Wolfe, S. *J. Am. Chem. Soc.* **1974**, *98*, 469.
(117) Del Bene, J. E. *J. Am. Chem. Soc.* **1978**, *100*, 1673.
(118) Downard, K. M.; Sheldon, J. C.; Bowie, J. H.; Lewis, D. E.; Hayes, R. N. *J. Am. Chem. Soc.* **1989**, *111*, 8112.
(119) Smith, B. J.; Radom, L. *J. Am. Chem. Soc.* **1993**, *115*, 4885.
(120) Förgeteg, S.; Bérces, T. *Acta Chim. Acad. Sci., Hung.* **1967**, *51*, 205.
(121) Bendakizzu, G. L.; Palmieri, P.; Pedulli, G. F. *Chem. Phys. Lett.* **1974**, *29*, 123.
(122) Whangbo, M. H.; Wolfe, S.; Bernardi, F. *Can. J. Chem.* **1975**, *53*, 3040.
(123) Lathan, W. A.; Curtiss, L. A.; Hehre, W. J.; Lilse, J. B.; Pople, J. A. *Progr. Phys. Org. Chem.* **1974**, *11*, 175.
(124) Sana, M.; Leroy, G. *J. Mol. Struct.* (*THEOCHEM*) **1991**, *226*, 307.
(125) Page, M.; Lin, M. C.; He, Y.; Choudhury, T. K. *J. Phys. Chem.* **1989**, *93*, 4404.

(126) Bouma, W. J.; Nobes, R. H.; Radom, L. *Org. Mass Spectrom.* **1982**, *17*, 845.

(127) Colwell, S. M. *Theor. Chem. Acta* **1988**, *74*, 123.

(128) Johnson, R. D., III; Tsai, B. P.; Hudgens, J. W. *J. Chem. Phys.* **1989**, *91*, 3340.

(129) Ashfold, M. N. R.; Howe, J. D. *Annu. Rev. Phys. Chem.* **1994**, *45*, 57.

(130) Ashfold, M. N. R.; Clement, S. G.; Howe, J. D.; Western, C. M. *J. Chem. Soc., Faraday Trans.* **1993**, *89*, 1153.

(131) Dyke, J. M.; Jonathan, N.; Mills, J. D.; Morris, A. *Mol. Phys.* **1980**, *40*, 1177.

(132) Burcat, A.; Kudchadker, S. *Acta Chim. Acad. Sci. Hung.* **1979**, *101*, 249.

(133) Frisch, M. J.; Trucks, G. W.; Schlegel, H. B.; Gill, P. M. W.; Johnson, B. G.; Wong, M. W.; Foresman, J. B.; Robb, M. A.; Head-Gordon, M.; Replogle, E. S.; Gomperts, R.; Andres, J. L.; Raghavachari, K.; Binkley, J. S.; Gonzalez, C.; Martin, R. L.; Fox, D. J.; Defrees, D. J.; Baker, J.; Stewart, J. J. P.; Pople, J. A. *Gaussian 92/DFT*, Revision G.1; Gaussian, Inc.: Pittsburgh, PA, 1993.

(134) Frisch, M. J.; Trucks, G. W.; Schlegel, H. B.; Gill, P. M. W.; Johnson, B. G.; Wong, M. W.; Foresman, J. B.; Robb, M. A.; Head-Gordon, M.; Replogle, E. S.; Gomperts, R.; Andres, J. L.; Raghavachari, K.; Binkley, J. S.; Gonzalez, C.; Martin, R. L.; Fox, D. J.; Defrees, D. J.; Baker, J.; Stewart, J. J. P.; Pople, J. A. *Gaussian 92/DFT*, Revision F.3; Gaussian, Inc.: Pittsburgh, PA, 1993.

(135) The numbering system we have adopted for hydroxymethyl species keeps the dominant mechanical action of each normal mode in the 3p Rydberg state (and cation) identical to the dominant mechanical action described by the same (numeric) mode in the ground state. This numbering system enables simple notation of electronic transitions and easy comparisons of frequencies. We also apply this normal mode numbering scheme for CH_2OH to the isotopically substituted species, even though isotopic substitution changes the energy order of the normal modes. The mode-numbering scheme used in this paper differs slightly from previous publications. Specifically, the ν_4 and ν_7 modes of refs 6 and 7 are the ν_7 and ν_4 modes of this paper, respectively. The ν_8 and ν_9 modes of refs 1, 2, 6, 7, and 100 are the ν_9 and ν_8 modes of this paper, respectively.

(136) Marston, C. C.; Balint-Kurti, G. G. *J. Chem. Phys.* **1989**, *91*, 3571.

(137) The harmonic frequencies for CH_2OH^+ reported by GAUSSIAN 92 and scaled by 0.97 are $\nu_8 = 1027$ cm^{-1} and $\nu_9 = 1234$ cm^{-1}.

(138) The harmonic frequencies for the CH_2OH radical reported by GAUSSIAN 92 and scaled by 0.94 are $\nu_8 = 417$ cm^{-1} and $\nu_9 = 607$ cm^{-1}.

(139) Montgomery, J. A. J.; Ochterski, J. W.; Petersson, G. A. *J. Chem. Phys.* **1994**, *101*, 5900.

(140) Hehre, W. J.; Ditchfield, R.; Radom, L.; Pople, J. A. *J. Am. Chem. Soc.* **1970**, *92*, 4796.

(141) Shimanouchi, T. *Table of Molecular Vibrational Frequencies*,-NSRDS-NBS-39; Dept. of Commerce, National Institute of Standards.

(142) Jacox, M. E.; Dal-Favero, M. E. *NIST Vibrational and Electronic Energy Levels Database*; Standard Reference Data: Gaithersburg, 1993; Vol. NIST Standard Database 26.

(143) Xu, L.-H.; Hougen, J. T. *J. Mol. Spectrosc.* **1995**, *173*, 540.

(144) All uncertainties presented in this paper represents one standard deviation, i.e., 1σ.

(145) Johnson, R. D., III; Tsai, B. P.; Hudgens, J. W. *J. Chem. Phys.* **1988**, *89*, 4558.

(146) Certain commercial materials and equipment are identified in this paper in order to adequately specify the experimental procedure. In no case does such identification imply recommendation or endorsement by the National Institute of Standards and Technology, nor does it imply that the material or equipment identified is the best available for the purpose.

(147) Tjossem, P. J. H.; Cool, T. A.; Webb, D. A.; Grant, E. R. *J. Chem. Phys.* **1988**, *88*, 617.

(148) Hudgens, J. W.; Dulcey, C. S.; Long, G. R.; Bogan, D. J. *J. Chem. Phys.* **1987**, *87*, 4546.

(149) Hudgens, J. W.; Johnson, R. D., III. *J. Phys. Chem.* **1987**, *91*, 6189.

(150) Irikura, K. K.; Hudgens, J. W.; Johnson, R. D., III. *J. Chem. Phys.* **1995**, *103*, 1303.

(151) Chase, M. W., Jr.; Davies, C. A.; Downey, J. R., Jr.; Frurip, D. J.; McDonald, R. A.; Syverud, A. N. *J. Phys. Chem. Ref. Data, Suppl.* **1985**, *14*.

(152) Gurvich, L. V.; Veits, I. V.; Medvedev, V. A.; Khachkuruzov, G. A.; Yungman, V. S.; Bergman, G. A. e. a. "*Termodinamicheskie Svoistva Individual'nykh Veshchestv*", (*Thermodynamic Properties of Individual Substances*); Izdatel'stov "Nauka": Moscow, 1979; Vol. 2.

(153) Lias, S. G.; Bartmess, J. E.; Holmes, J. L.; Levin, R. D.; Liebman, J. F.; Mallard, G. *J. Phys. Chem. Ref. Data* (*Suppl. Ser. 1*) **1988**, *17*.

(154) Heath, R. L. Table of the Isotopes. In *CRC Handbook of Chemistry and Physics*, 64 ed.; Weast, R. C., Astle, M. J. H. B. W., Eds.; CRC Press, Inc.: Boca Raton, 1984.

(155) Mayer, J. E.; Brunauer, S.; Mayer, M. G. *J. Am. Chem. Soc.* **1933**, *55*, 37.

(156) Benson, S. W. *Thermochemical Kinetics*, 2nd ed.; John Wiley & Sons: New York, 1976; pp 47−50.

(157) Bunker, P. R. *Molecular Symmetry and Spectroscopy*; Academic Press: New York, 1979.

(158) Herzberg, G. *Proc. R. Soc. London Ser. A* **1961**, *262*, 291.

(159) Habenicht, W.; Reiser, G.; Müller-Dethlefs, K. *J. Chem. Phys.* **1991**, *95*, 4809.

(160) Bevington, P. R. *Data Reduction and Error Analysis for the Physical Sciencies*; McGraw-Hill Book Co.: New York, 1969.

(161) A presumption of these extrapolations to 0 K is that the products and reactants are at 298 K. Since this fact is not measured, the possibility that the products are at an arbitrary temperature adds to the uncertainty of the appearance energy. In this discussion we have not accounted for this uncertainty explicity.

(162) For these derivations thermochemical properties e^-, H^+, H, OH, OH^+, H_2, Cl, Br, I, HCl, HBr, HI, CO, CH_4, and CH_3 were obtained from ref 151. Thermochemical properties of CH_3OH, CH_3CH_2OH, and CH_2O were obtained from ref 163.

(163) *TRC Thermodynamic Tables−Nonhydrocarbons*; The Texas A&M University System, December 31, 1986.

JP961399+